Structural Variation in Cerium Aryloxide Complexes Templated by Hemilabile K^+-Amine Interactions

Jee Eon Kim, Patrick J. Carroll, and Eric J. Schelter*

P. Roy and Diana T. Vagelos Laboratories, Department of Chemistry, University of Pennsylvania, Philadelphia, PA 19104

E-mail: schelter@sas.upenn.edu

Supporting Information

Figure S1. ^{1}H- and ^{19}F-NMR spectra of K[Ce(OTf)(bdmmp)$_3$] (**1**) S3

Figure S2. ^{1}H-, ^{19}F-NMR and ^{13}C NMR spectra of K[La(OTf)(bdmmp)$_3$] (**1–La**) S4–S5

Figure S3. ^{1}H-NMR spectra of K[Ce(OC$_6$H$_5$)(bdmmp)$_3$] (**2**) in benzene-d_6, methylene chloride-d_2 . S6

Figure S4. ^{1}H-NMR spectrum of K[Ce(OC$_6$H$_5$)(bdmmp)$_3$] (**2**) in toluene-d_8 ..... S7

Figure S5. VT NMR spectra of K[Ce(OC$_6$H$_5$)(bdmmp)$_3$] (**2**) and chemical shift-temperature plot S8

Figure S6. ^{1}H NMR spectrum of Ce(OC$_{10}$H$_7$)(bdmmp)$_3$K (**3**) in benzene-d_6 and methylene chloride-d$_2$ at 300 K S9

Figure S7. ^{1}H NMR spectrum of K[Ce(OC$_{10}$H$_7$)(bdmmp)$_3$] (**3**) in toluene-d_8. ..... S10

Figure S8. ^{1}H NMR and ^{13}C NMR spectra of K[La(OC$_{10}$H$_7$)(bdmmp)$_3$] (**3–La**) in toluene-d_8. ..... S11

Figure S9. VT NMR spectra of K[Ce(OC$_{10}$H$_7$)(bdmmp)$_3$] (**3**) and chemical shift-temperature plot S12

Figure S10. ^{1}H NMR spectrum of K[Ce(OC$_6$H$_3$-2,4-*t*Bu)(bdmmp)$_3$] (**4**) in benzene-d_6 at 300 K S13

Figure S11. ^{1}H NMR spectrum of K[Ce(OC$_6$H$_3$-2,4-*t*Bu)(bdmmp)$_3$] (**4**) in methylene chloride-d_2 at 300K S13

Figure S12. ^{1}H- and ^{13}C NMR spectra of K[La(OC$_6$H$_3$-2,4-*t*Bu)(bdmmp)$_3$] (**4–La**) in toluene-d_8 .... S14

Figure S13. VT NMR spectrum of K[Ce(OC$_6$H$_3$-2,4-*t*Bu)(bdmmp)$_3$] (**4**) in toluene-d_8 from 300–370 K S15

Figure S14. ^{1}H NMR spectrum of K[Ce(OC$_6$H$_3$-2,4-*t*Bu)(bdmmp)$_3$] (**4**) in toluene-d_8 at 370 K S16

Figure S15. ^{1}H NMR spectrum of K[Ce(OC$_6$H$_3$-2,6-Ph)(bdmmp)$_3$] (**5**) in benzene-d_6 and methylene chloride-d_2 at 300 K S17

Figure S16. ^{1}H- and ^{13}C NMR spectra of K[La(OC$_6$H$_3$-2,6-Ph)(bdmmp)$_3$] (**5-La**) in benzene-d_6 ..... S18

Figure S17. VT NMR spectrum of K[Ce(OC$_6$H$_3$-2,6-Ph)(bdmmp)$_3$] (**5**) in toluene-d_8 from 300–370 K S19

Figure S18. ^{1}H NMR spectrum of K[Ce(OC$_6$H$_3$-2,6-Ph)(bdmmp)$_3$] (**5**) in toluene-d_8 at 370 K S20

Figure S19. Thermal Ellipsoid Plot of K[Ce(OTf)(bdmmp)$_3$] (**1**) S21

Figure S20. Thermal Ellipsoid Plot of K[Ce(OC$_6$H$_5$)(bdmmp)$_3$] (**2**) S22

Figure S21. Thermal Ellipsoid Plot of K[Ce($OC_{10}H_7$)(bdmmp)$_3$] (**3**).....S23
Figure S22. Thermal Ellipsoid Plot of K[Ce(OC_6H_3-2,4-*t*Bu)(bdmmp)$_3$] (**4**).....S24
Figure S23. Thermal Ellipsoid Plot of K[Ce(OC_6H_3-2,6-Ph)(bdmmp)$_3$] (**5**) S25
Figure S24. Thermal Ellipsoid Plot of K[Ce(O*t*Bu)(bdmmp)$_3$] (**6**) S26
Figure S25. Thermal Ellipsoid Plot of K[Ce(OC_6H_3-2,6-*i*Pr)$_2$(bdmmp)$_2$] (**7**) S27
Figure S26. Thermal Ellipsoid Plot of K[Ce(OH)(bdmmp)$_3$] (**8**) S28
Figure S27. Electrochemical Analysis of K[Ce(OC_6H_5)(bdmmp)$_3$] (**2**) S29
Figure S28. Electrochemical Analysis of K[Ce($OC_{10}H_7$)(bdmmp)$_3$] (**3**) S30
Figure S29. Electrochemical Analysis of K[Ce(OC_6H_3-2,4-*t*Bu)(bdmmp)$_3$] (**4**) S31
Figure S30. Cyclic voltammograms of K[Ce(OC_6H_3-2,4-*t*Bu)(bdmmp)$_3$] (**4**) and K[La(OC_6H_3-2,4-*t*Bu)(bdmmp)$_3$] **(4–La)** S32
Figure S31. Electrochemical Analysis of K[Ce(OC_6H_3-2,6-Ph)(bdmmp)$_3$] (**3**).....S33
Figure S32. Cyclic voltammograms of K[Ce(OC_6H_3-2,6-Ph)(bdmmp)$_3$] (**5**) and K[La(OC_6H_3-2,6-Ph)(bdmmp)$_3$] **(5–La)** S34
Figure S33. ^{1}H NMR of K[Ce(O*t*Bu)(bdmmp)$_3$] (**6**) in benzene-d_6.....S35
Figure S34. ^{1}H NMR of K[Ce(OC_6H_3-2,6- *i*Pr)$_2$(bdmmp)$_2$] (**7**) in benzene-d_6.....S36
Figure S35. Decomposition of K[Ce(O*t*Bu)(bdmmp)$_3$] (**6**) to K[Ce(OH)(bdmmp)$_3$] (**8**) in glovebox S37
Figure S36. ^{1}H NMR of K[Ce(OH)(bdmmp)$_3$] (**8**) in benzene-d_6.....S38
Figure S37. Addition of degassed H_2O into K[Ce(O*t*Bu)(bdmmp)$_3$] (**6**) in benzene-d_6 in the J-young tube S39
Figure S38. IR spectrum of K[Ce(OH)(bdmmp)$_3$] (**8**) in KBr plate in Nujol S40
Figure S39. Cyclic voltammograms of K[Ce(OH)(bdmmp)$_3$] (**8**) S41
Table 1. Table S1. Summary of structural determination of compound **1**–**4**.....S42
Table 2. Table S1. Summary of structural determination of compound **5**–**8**.....S43

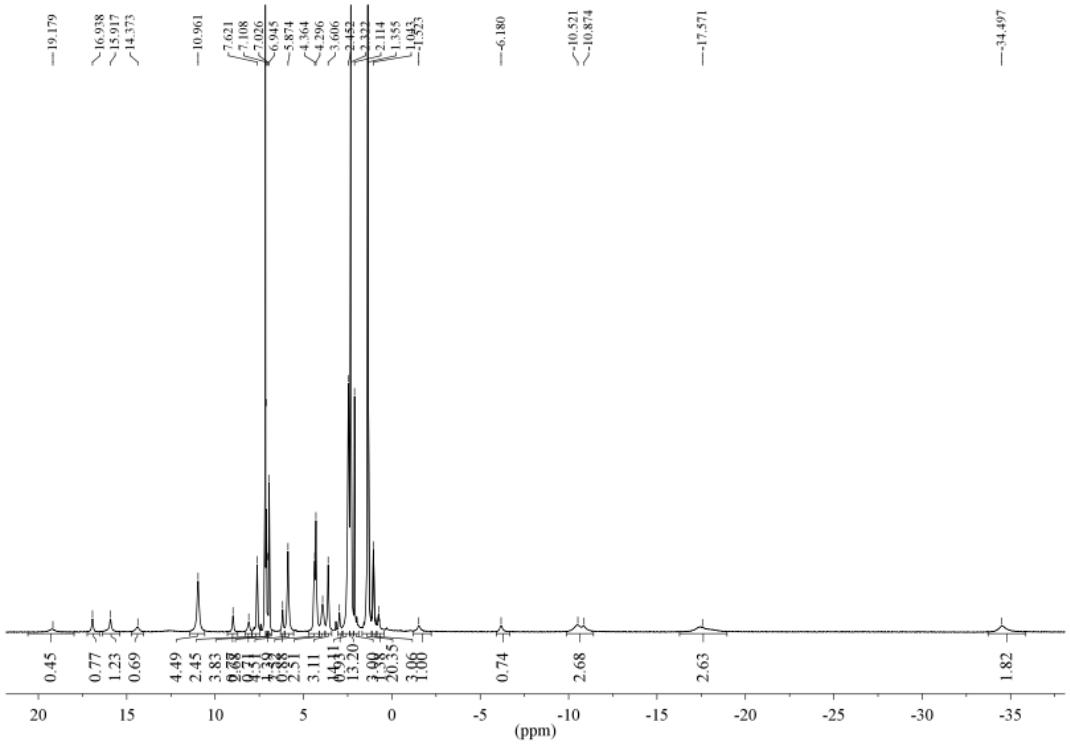

Figure S1a. ^{1}H NMR spectra for K[Ce(OTf)(bdmmp)$_3$] **(1)** in benzene-d_6.

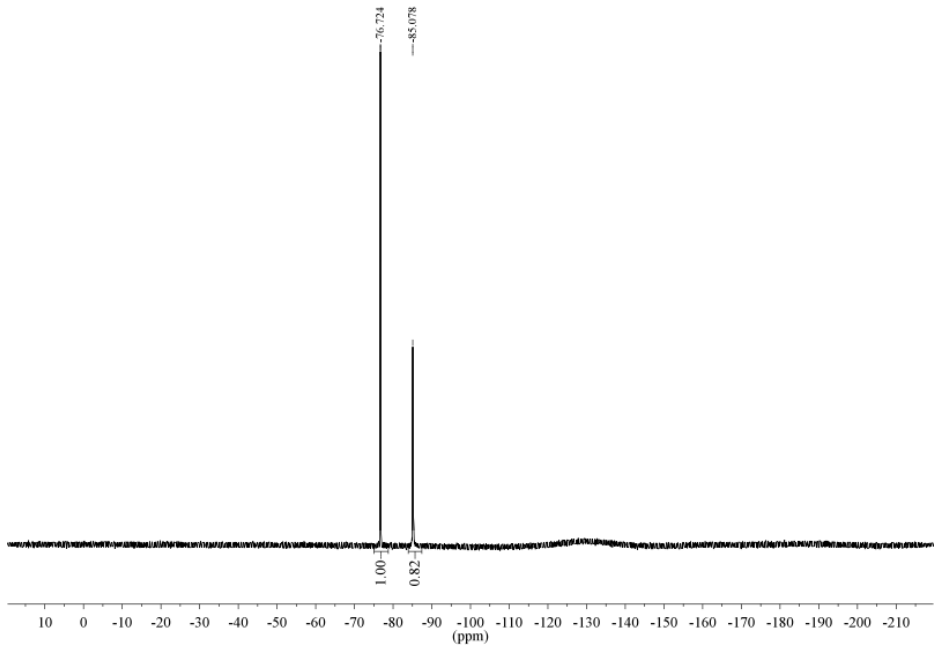

Figure S1b. ^{19}F NMR spectra for K[Ce(OTf)(bdmmp)$_3$] **(1)** in benzene-d_6

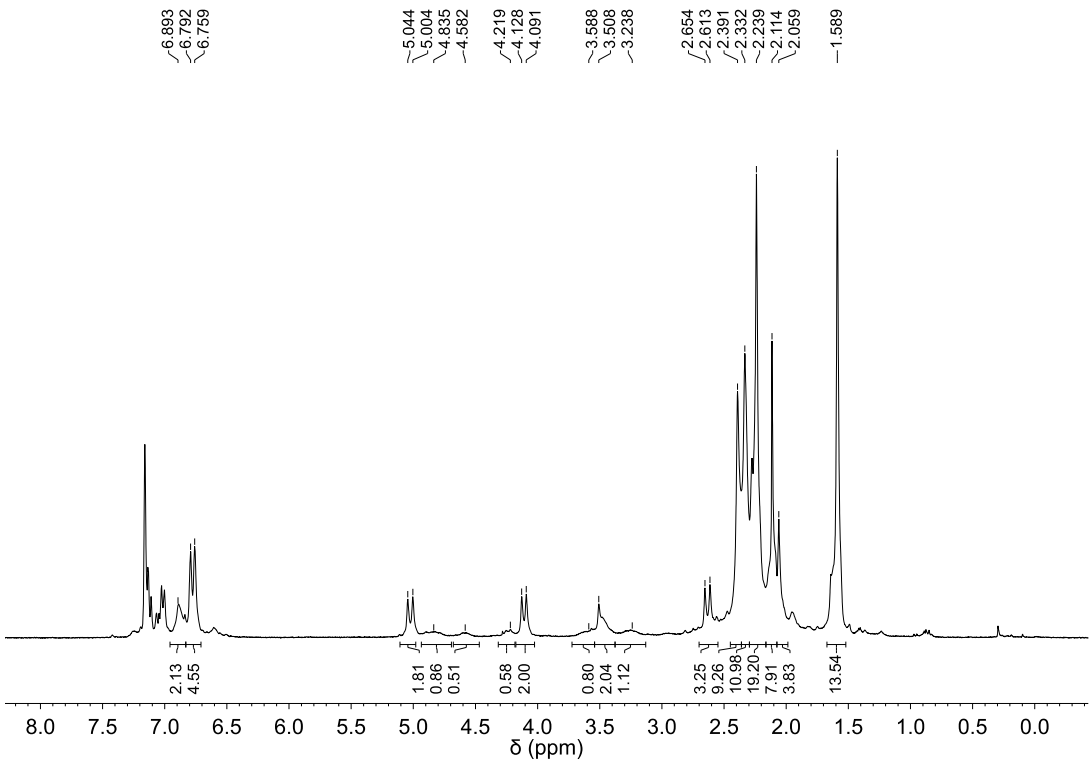

Figure S2a. ^{1}H NMR spectrum of K[La(OTf)(bdmmp)$_3$] (**1–La**) in benzene-d_6.

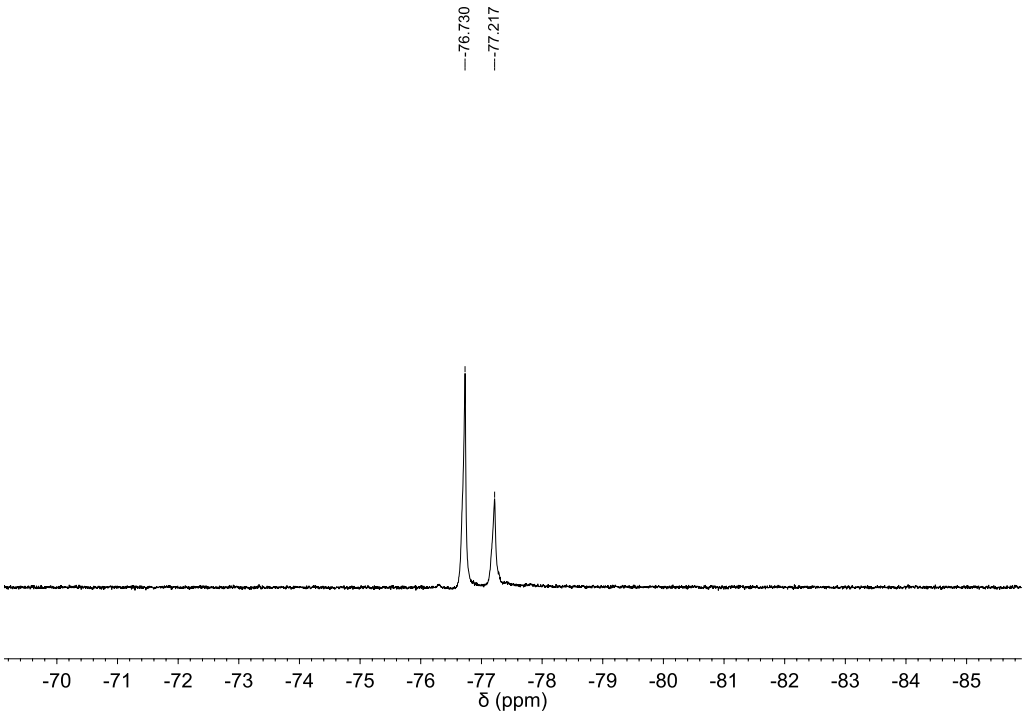

Figure S2b. ^{19}F NMR spectrum of K[La(OTf)(bdmmp)$_3$] (**1–La**) in benzene-d_6.

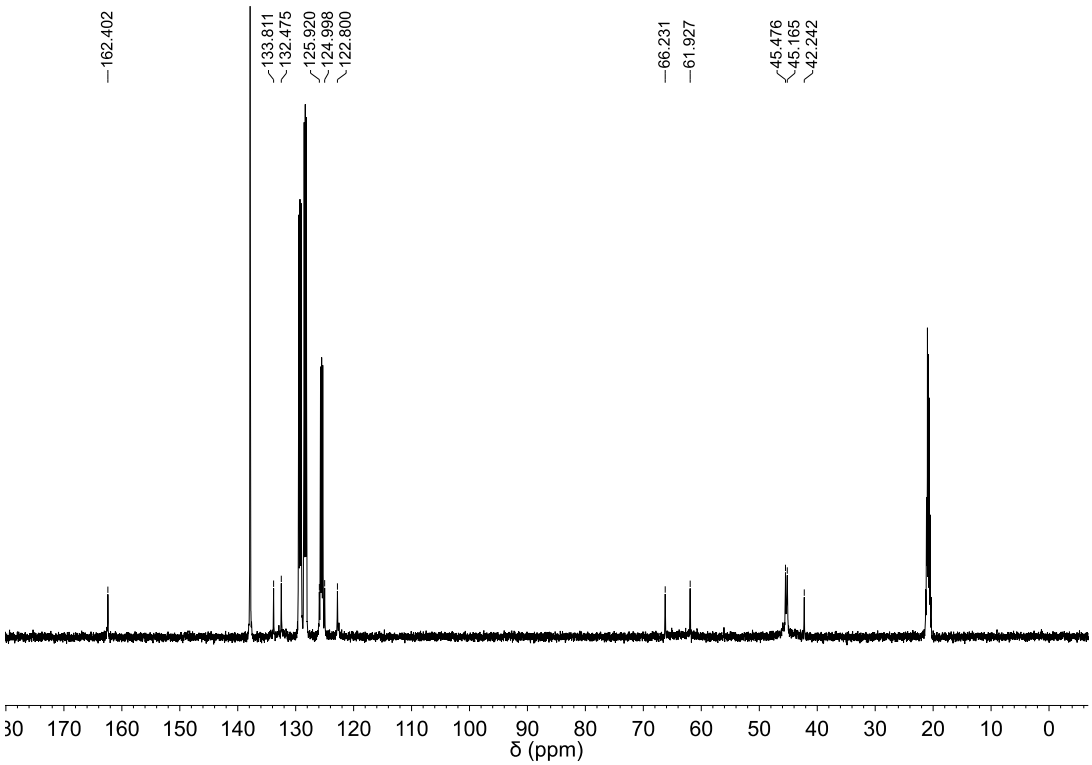

Figure S2c. ^{13}C NMR spectrum of K[La(OTf)(bdmmp)$_3$] (**1–La**) in toluene-d_8.

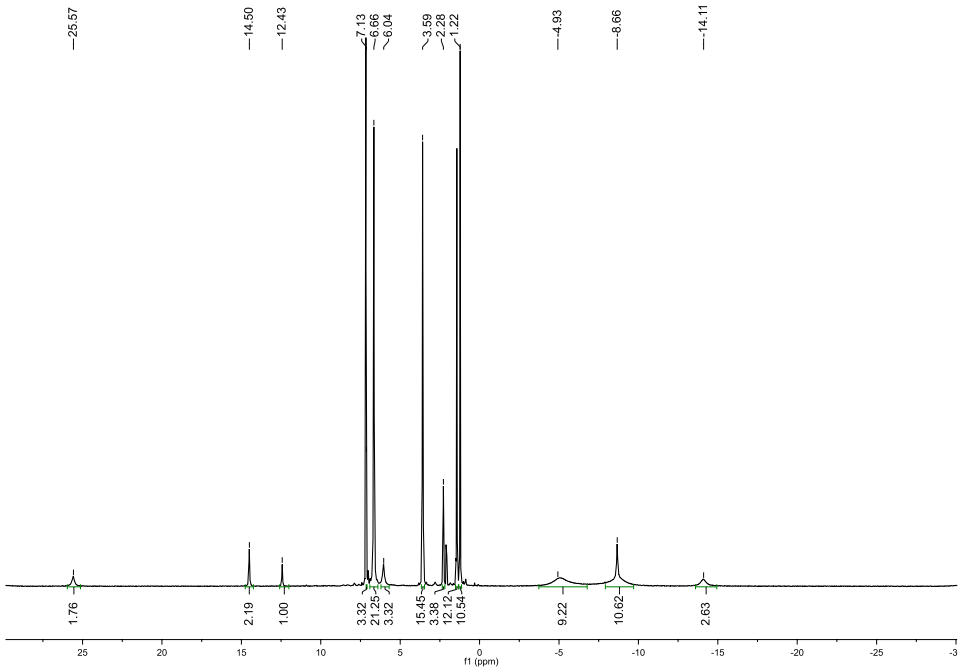

Figure S3a. ^{1}H NMR spectra for $Ce(OC_6H_5)(bdmmp)_3K$ **(2)** in benzene-d_6.

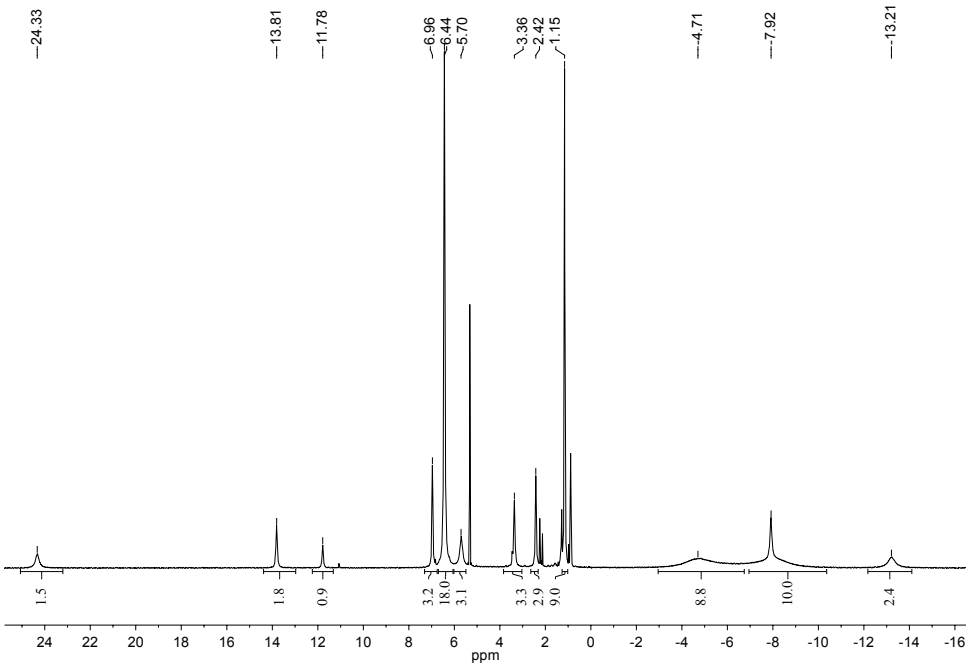

Figure S3b. ^{1}H NMR spectra for $Ce(OC_6H_5)(bdmmp)_3K$ **(2)** in methylene chloride-d_2.

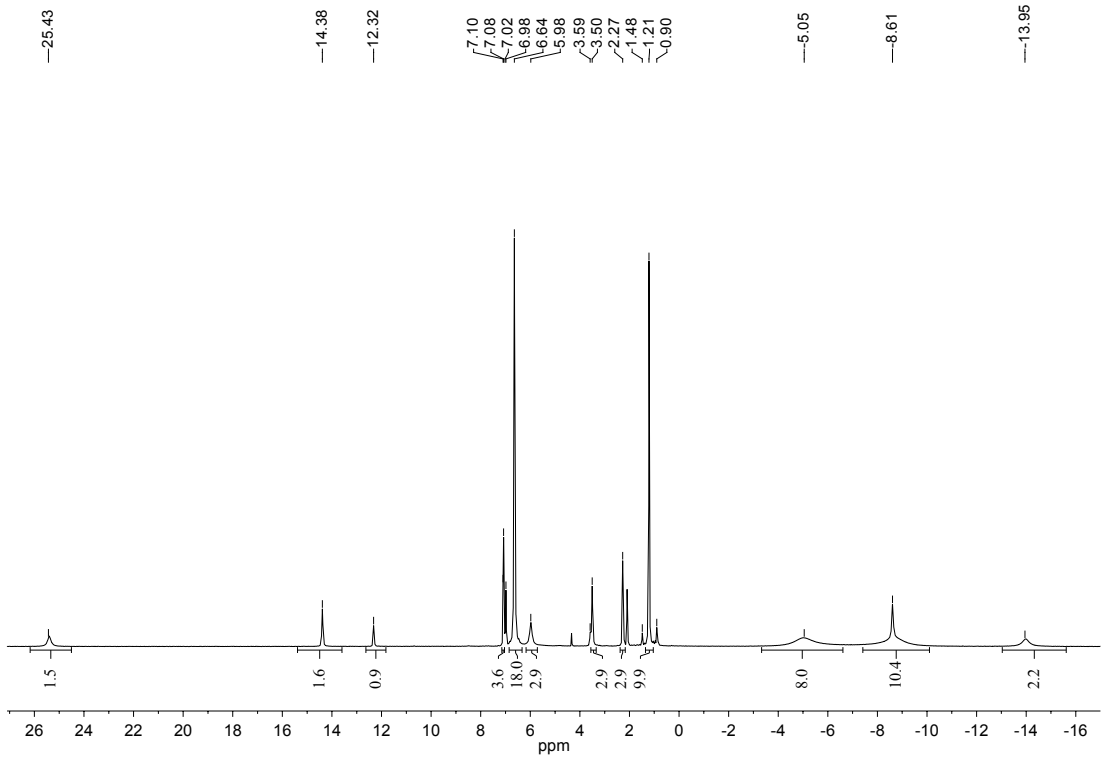

Figure S4. ^{1}H NMR spectra for $Ce(OC_6H_5)(bdmmp)_3K$ **(2)** in toluene-d_8.

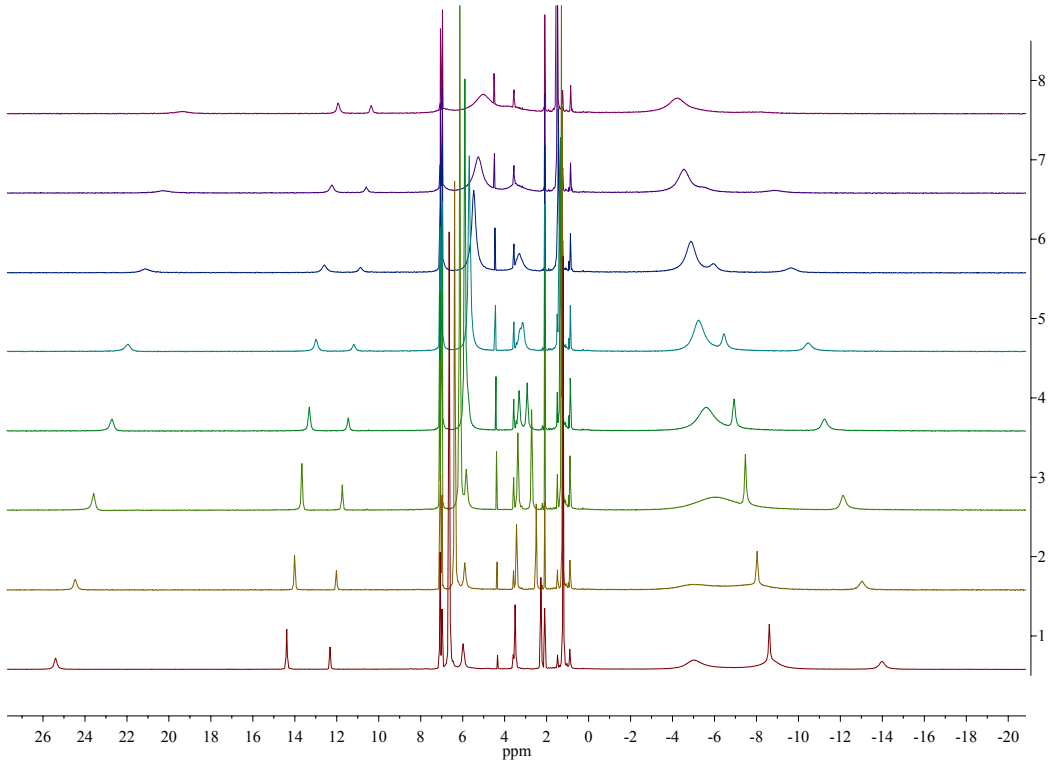

Figure S5a. VT NMR of $K[Ce(OC_6H_5)(bdmmp)_3]$ in toluene-d_8 from 300–370 K.

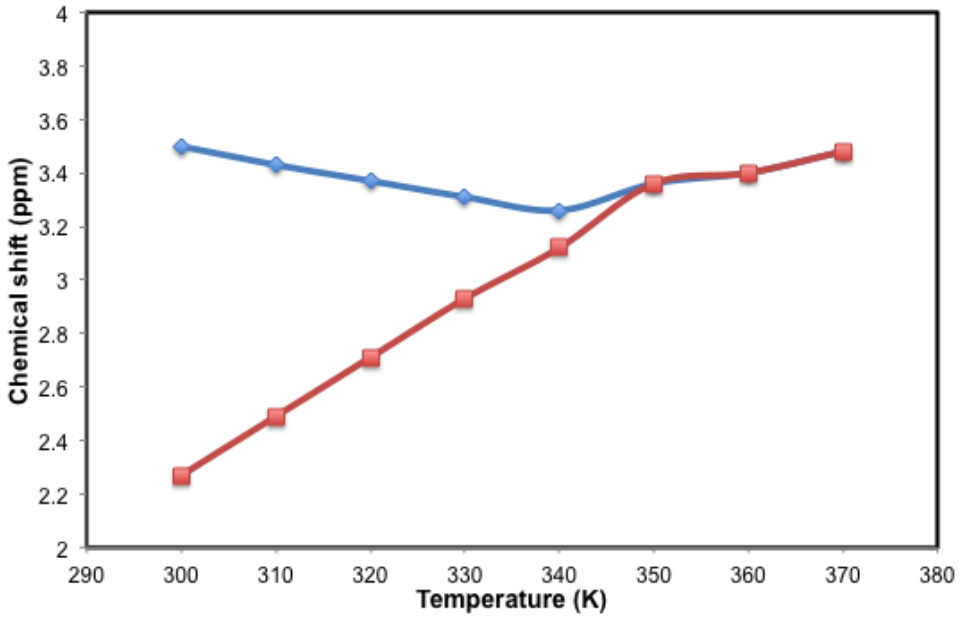

Figure S5b. Chemical shift (ppm) versus temperature (K) plot of $K[Ce(OC_6H_5)(bdmmp)_3]$ (**2**).

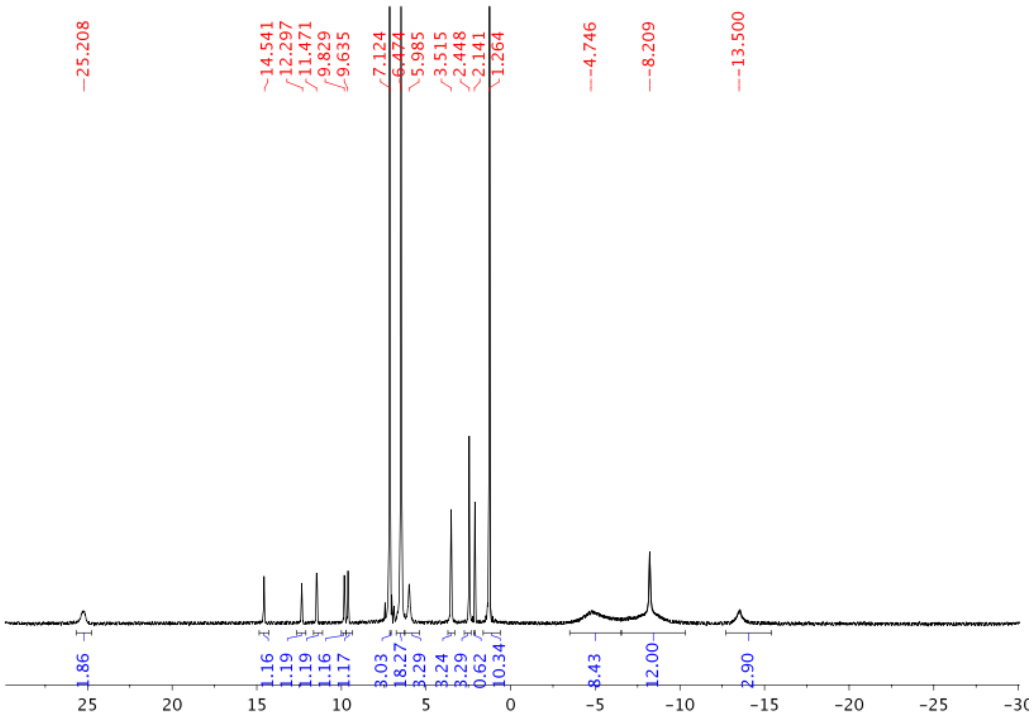

Figure S6a. ^{1}H NMR spectra for $Ce(OC_{10}H_7)(bdmmp)_3K$ (**3**) in benzene-d_6.

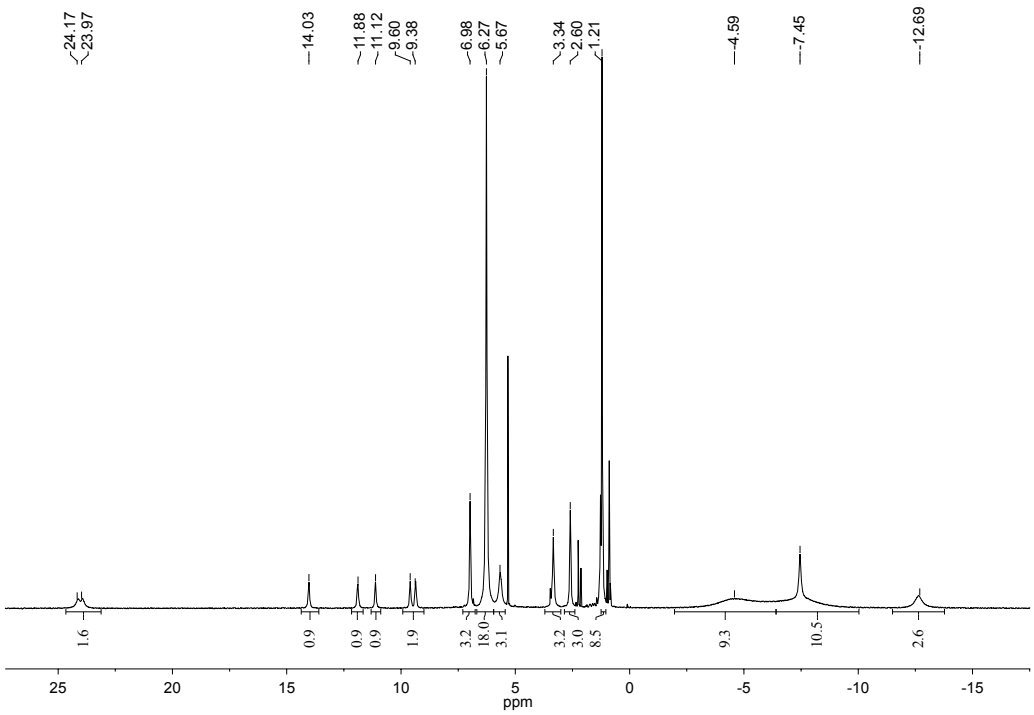

Figure S6b. ^{1}H NMR spectra for $Ce(OC_{10}H_7)(bdmmp)_3K$ (**3**) in methylene chloride-d_2.

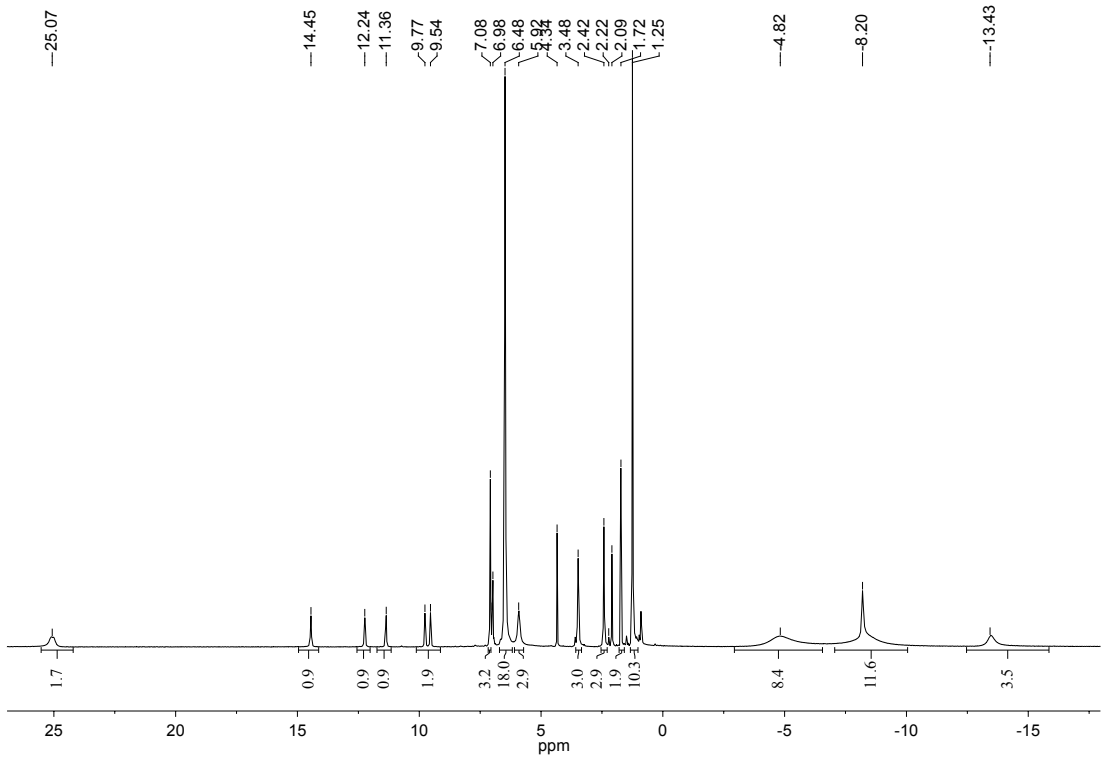

Figure S7. ^{1}H NMR spectra for $Ce(OC_{10}H_7)(bdmmp)_3K$ (**3**) in toluene-d_8.

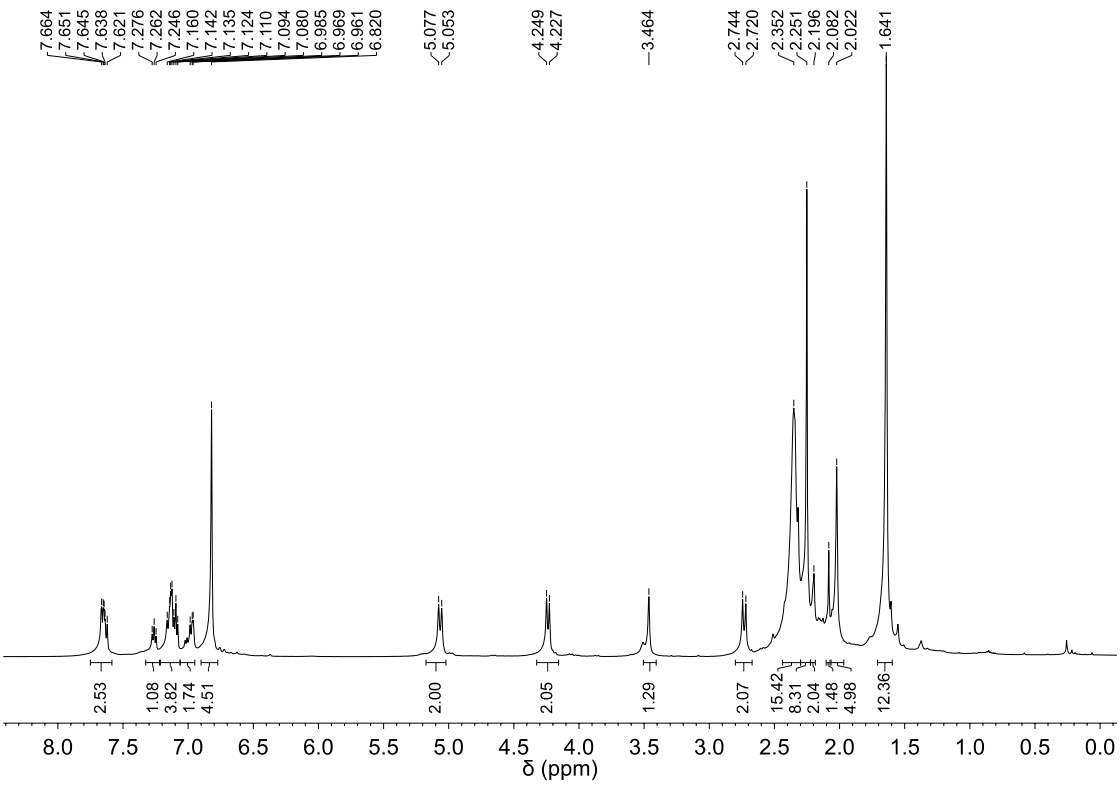

Figure S8a. ^{1}H NMR spectrum of K[La(OC$_{10}$H$_{7}$)(bdmmp)$_{3}$] (**3–La**) in benzene-d_6.

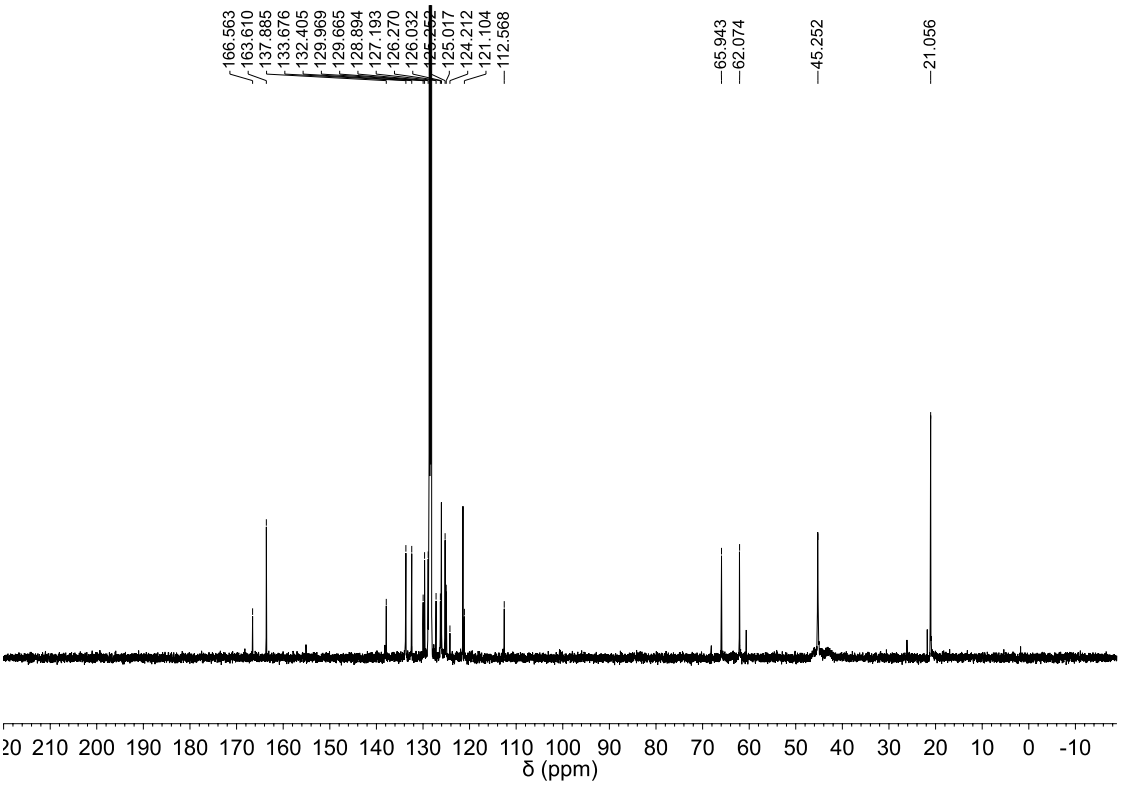

Figure S8b. ^{13}C NMR spectrum of K[La(OC$_{10}$H$_{7}$)(bdmmp)$_{3}$] (**3–La**) in benzene-d_6

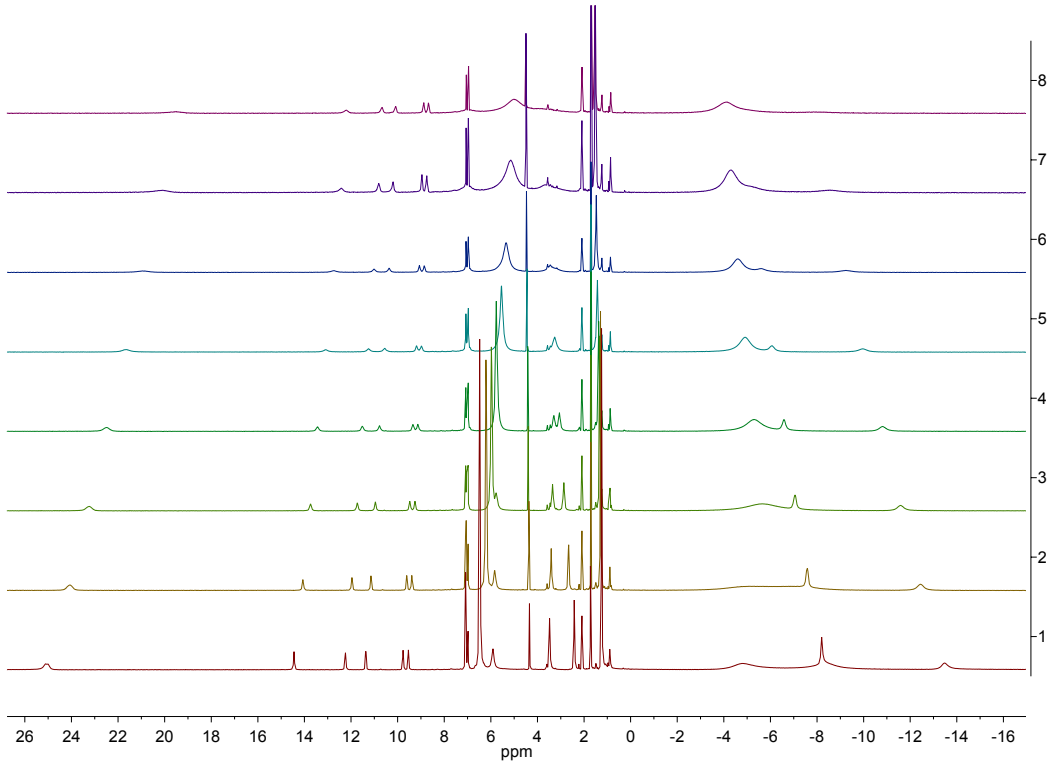

Figure S9a. VT NMR of K[Ce($OC_{10}H_7$)(bdmmp)$_3$] (**3**) in toluene-d_8 from 300–370 K.

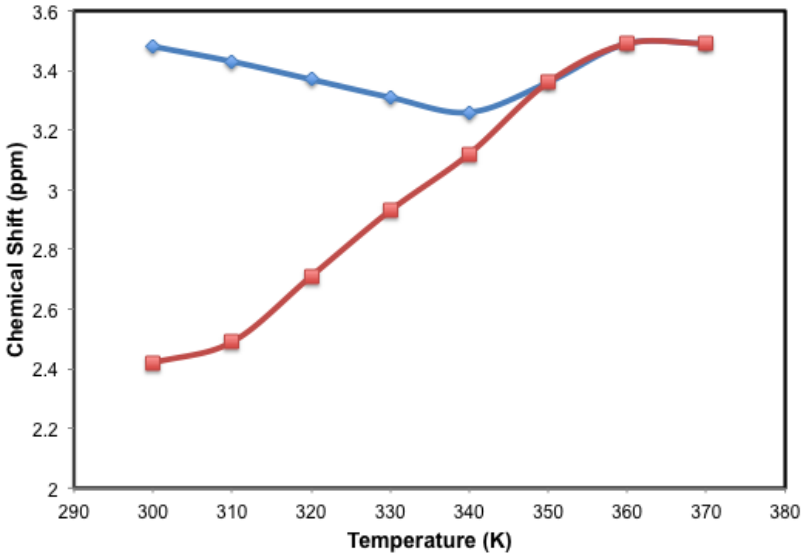

Figure S9b. Chemical shift (ppm) versus temperature (K) plot of K[Ce($OC_{10}H_7$)(bdmmp)$_3$] (**3**).

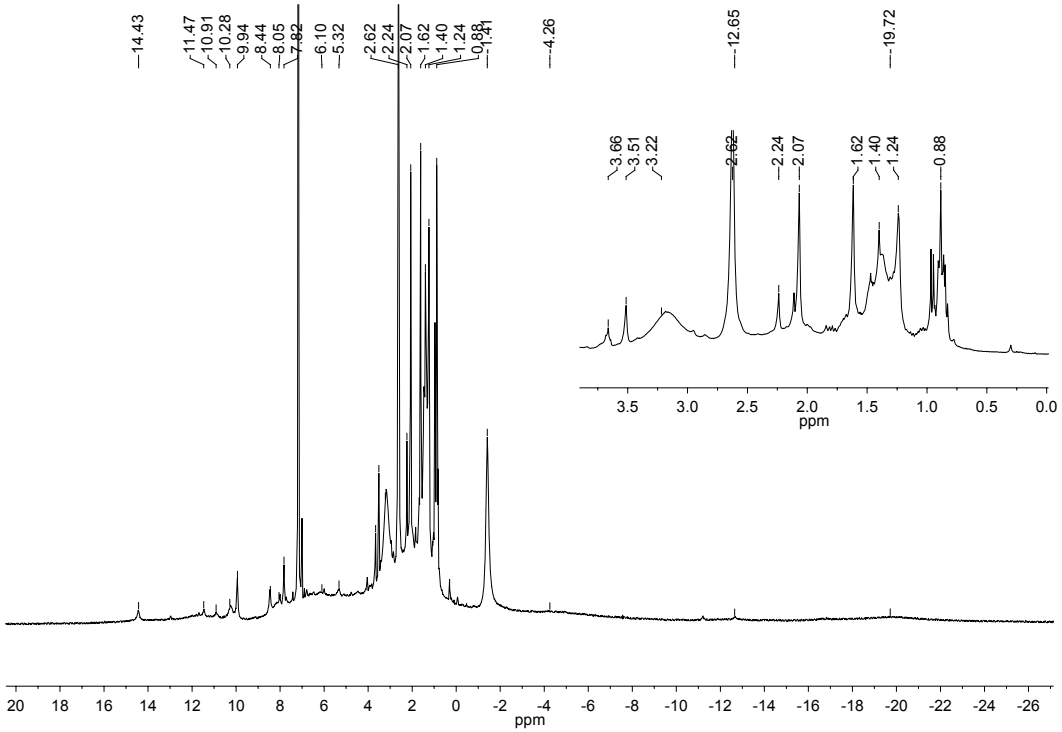

Figure S10. ^{1}H NMR spectrum of K[Ce(OC$_6$H$_3$-2,4-*t*Bu)(bdmmp)$_3$] (**4**) in benzene-d_6 at 300 K.

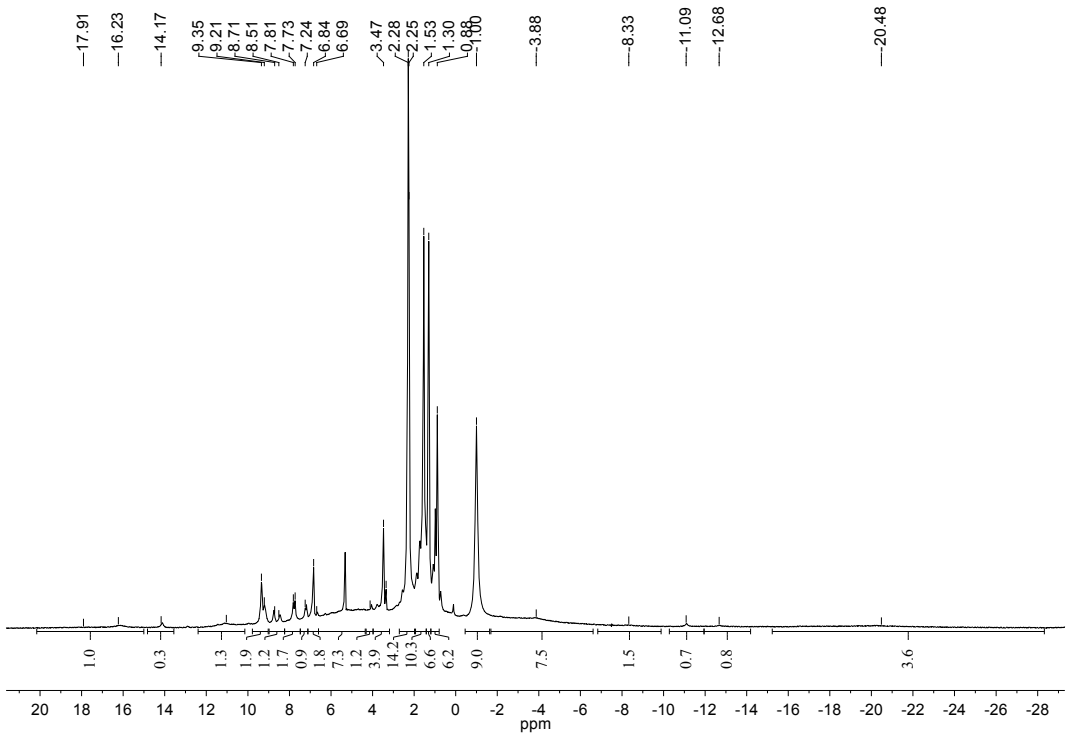

Figure S11. ^{1}H NMR spectrum of K[Ce(OC$_6$H$_3$-2,4-*t*Bu)(bdmmp)$_3$] (**4**) in methylene chloride-d$_2$ at 300 K.

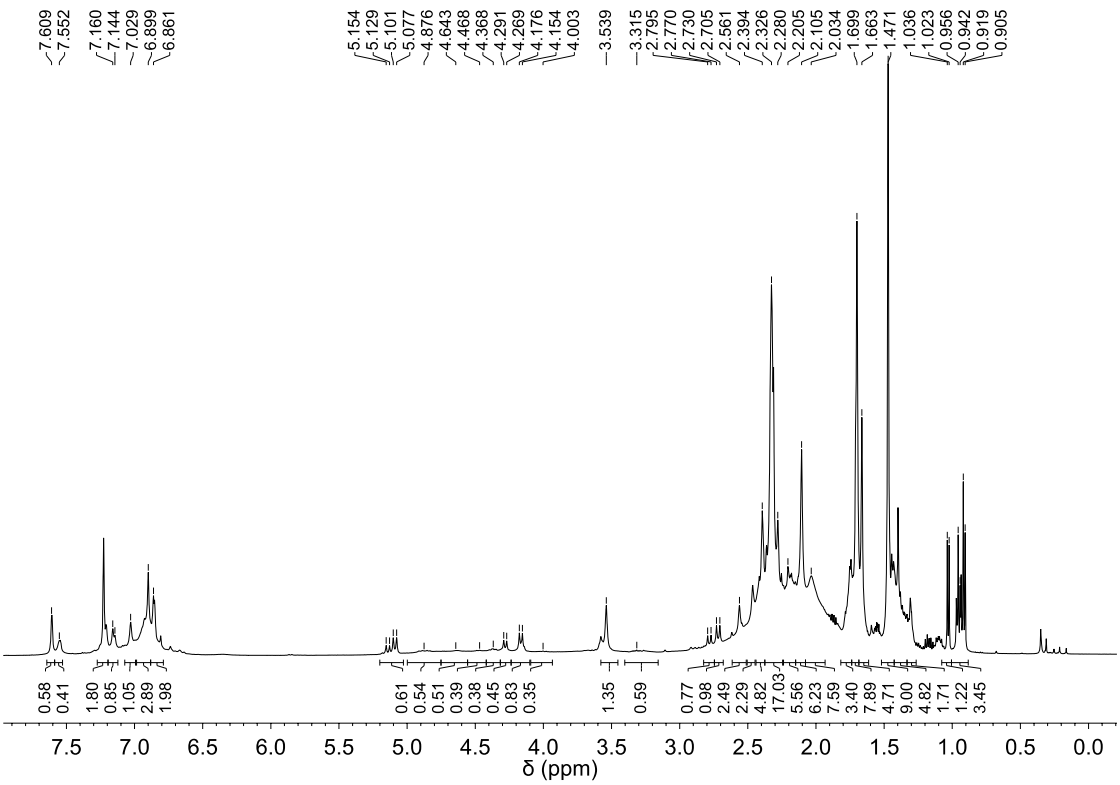

Figure S12a. ^{1}H NMR of K[La(OC_6H_3-2,4-*t*Bu)(bdmmp)$_3$] (**4–La**) in benzene-d_6.

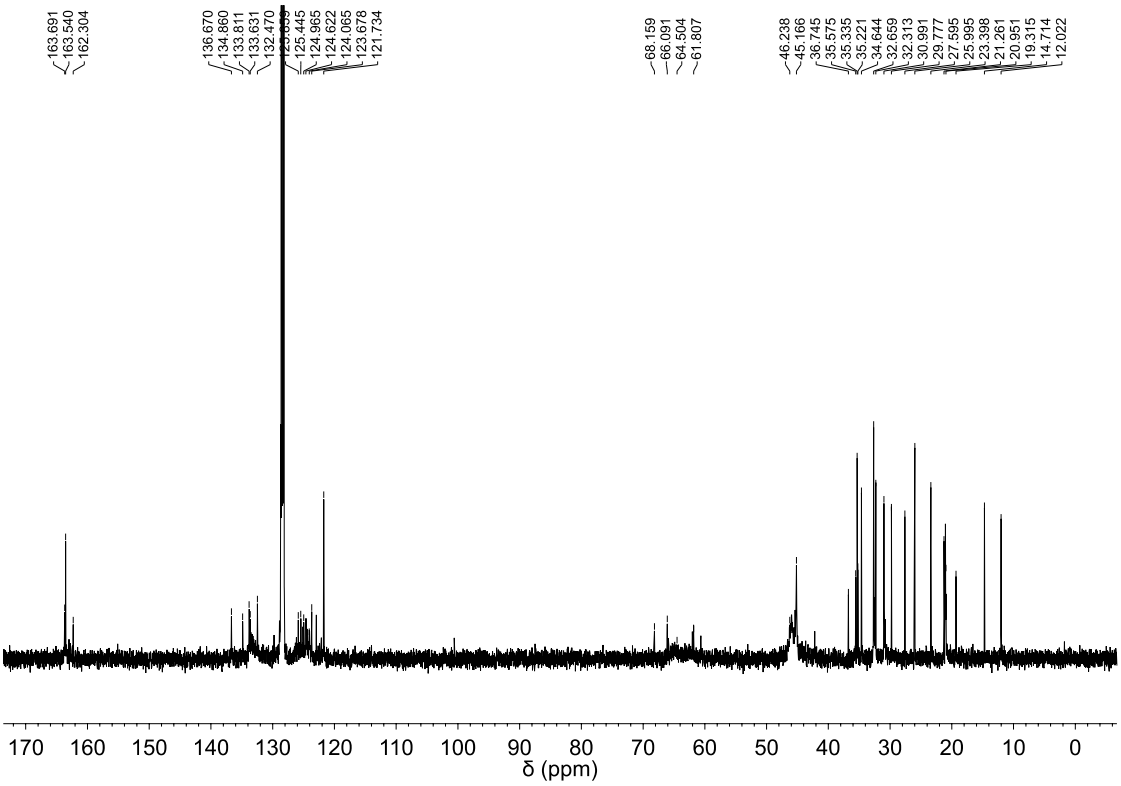

Figure S12b. ^{13}C NMR of K[La(OC_6H_3-2,4-*t*Bu)(bdmmp)$_3$] (**4–La**) in benzene-d_6.

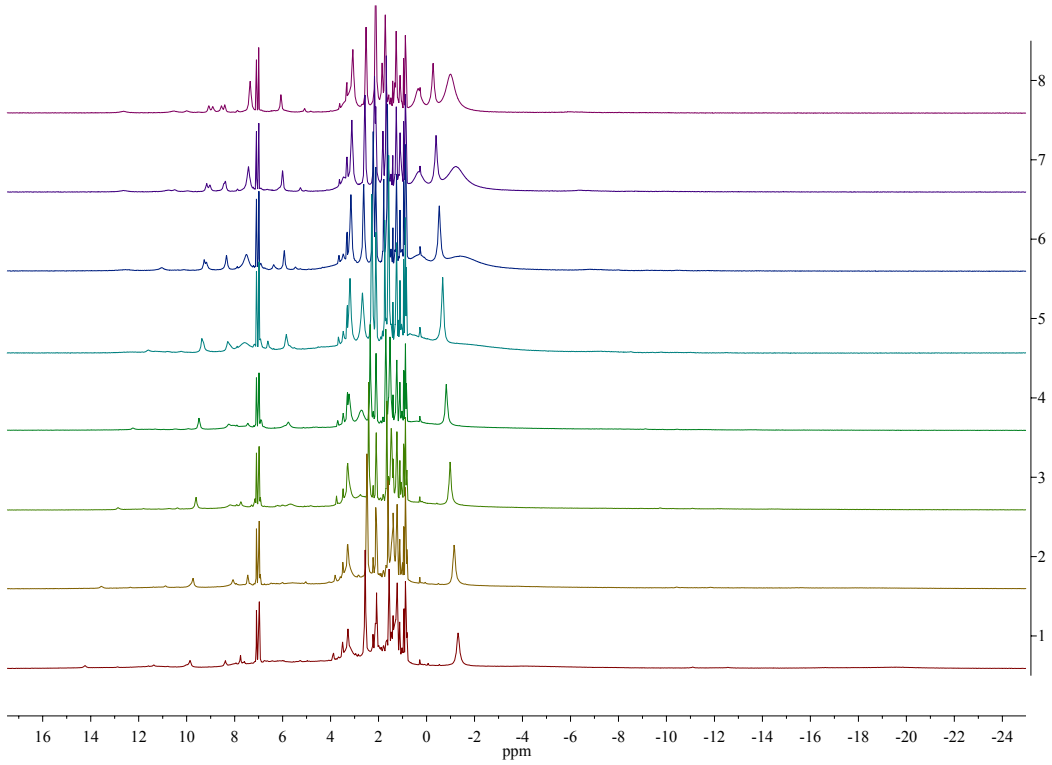

Figure S13. VT NMR of K[Ce(OC_6H_3-2,4-*t*Bu)(bdmmp)$_3$] (**4**) in toluene-d_8 from 300–370 K.

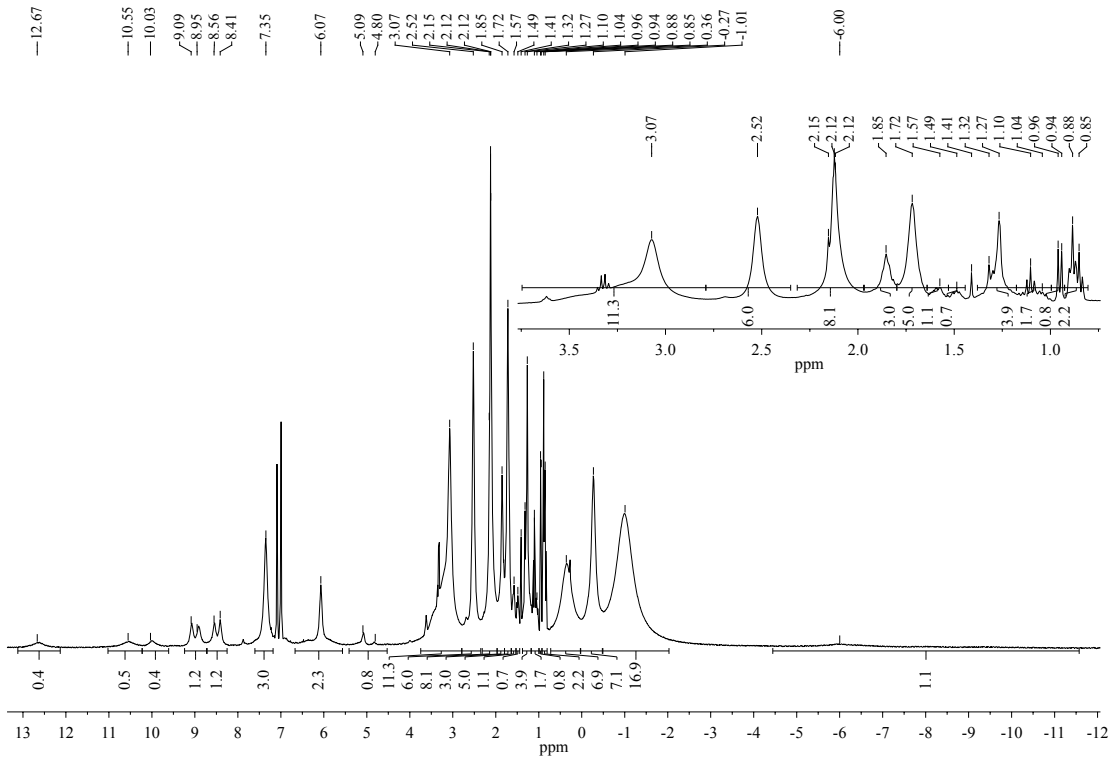

Figure S14. ^{1}H NMR spectrum of K[Ce(OC$_6$H$_3$-2,4-*t*Bu)(bdmmp)$_3$] (**4**) in toluene-d_8 at 370 K.

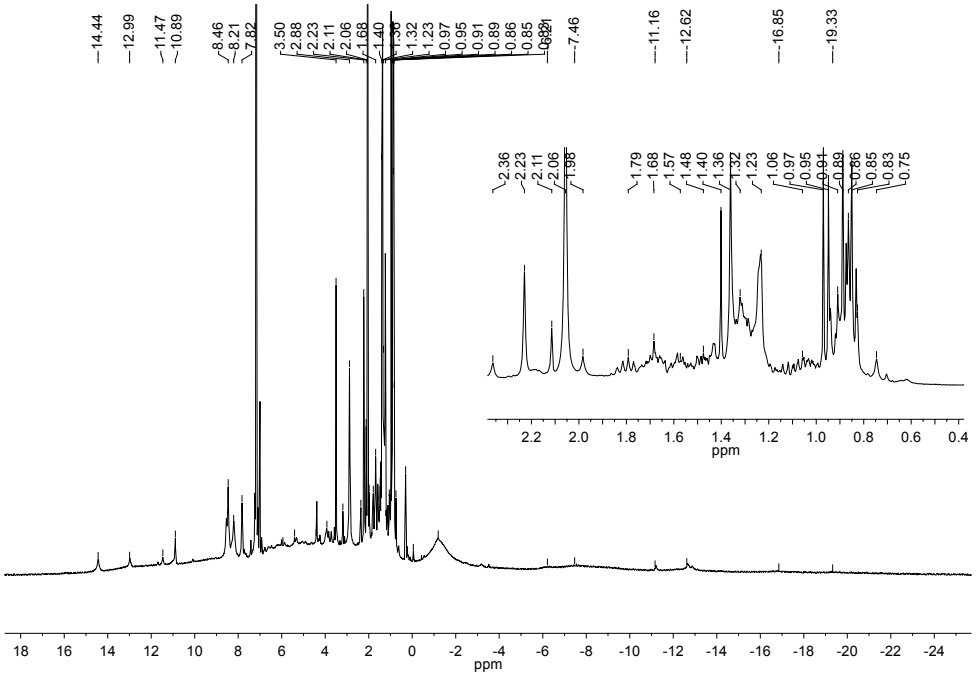

Figure S15a. ^{1}H NMR of K[Ce(OC_6H_3-2,6-Ph)(bdmmp)$_3$] (**5**) in benzene-d_6 at 300 K.

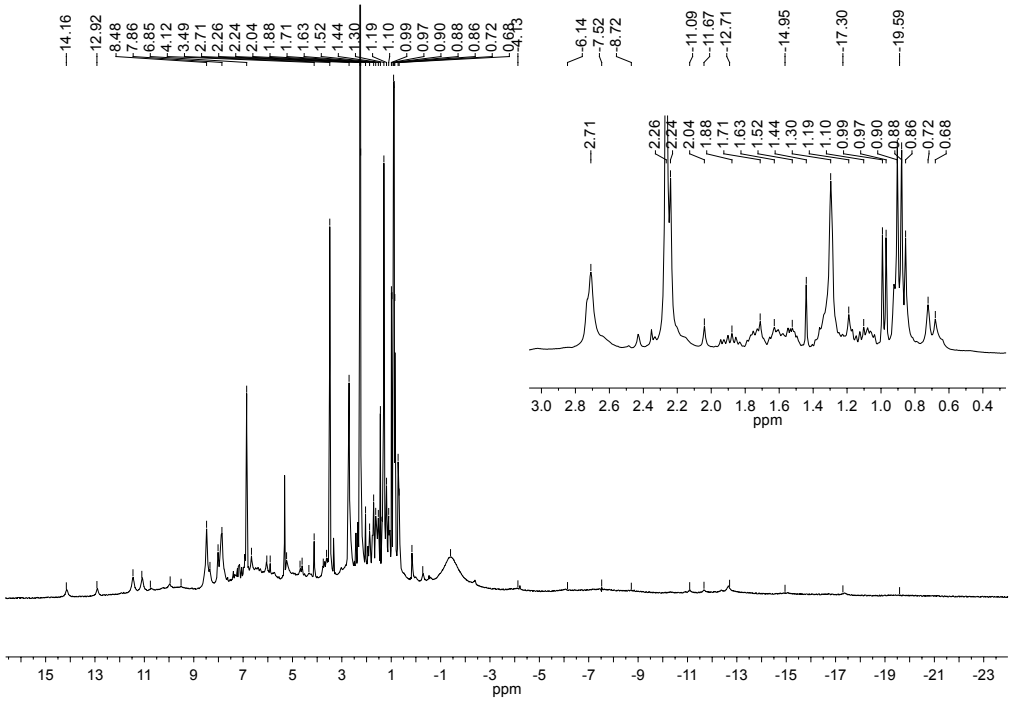

Figure S15b. ^{1}H NMR of K[Ce(OC_6H_3-2,6-Ph)(bdmmp)$_3$] (**5**) in methylene chloride-d_2 at 300 K.

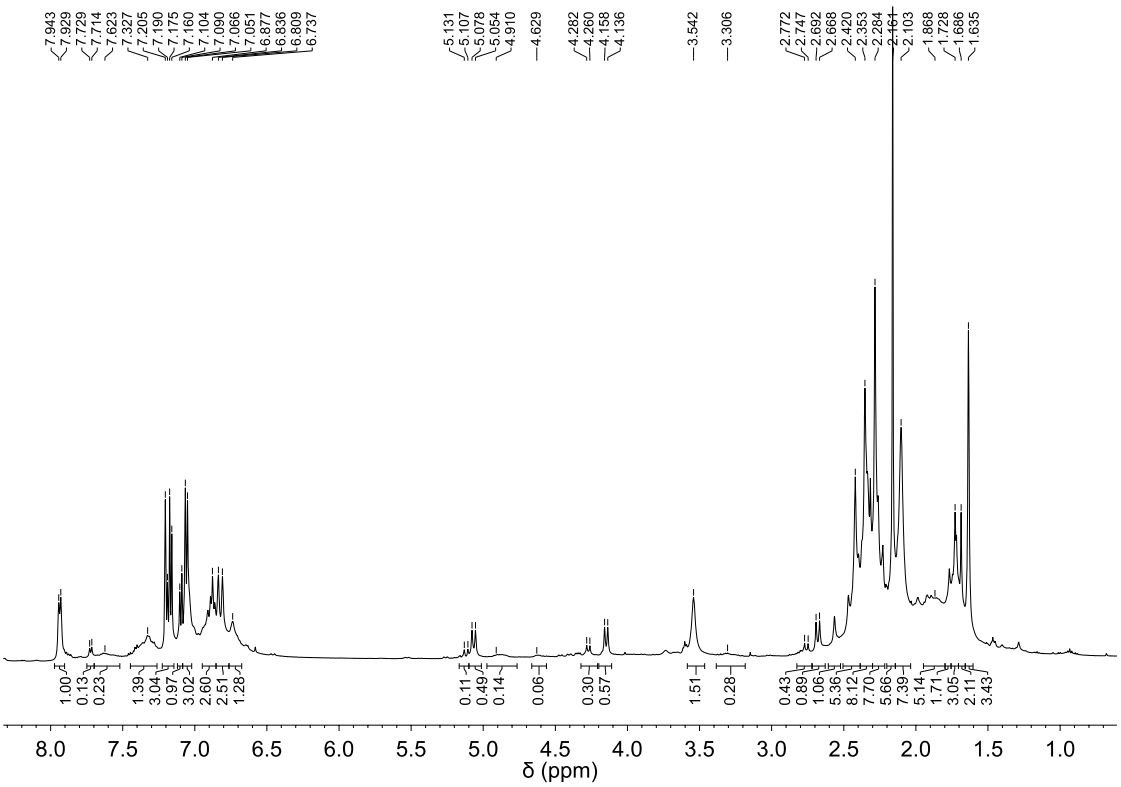

Figure S16a. ^{1}H NMR of K[La(OC$_6$H$_3$-2,6-Ph)(bdmmp)$_3$] (**5–La**) in benzene-d_6.

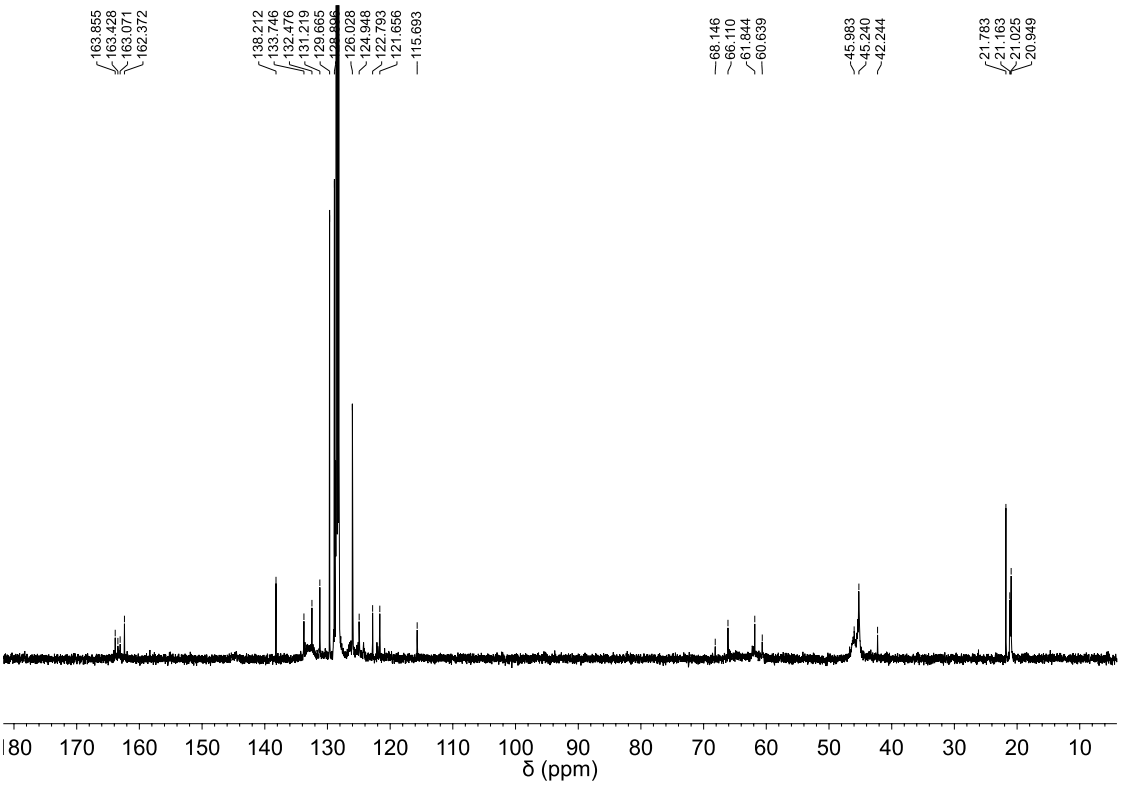

Figure S16b. ^{13}C NMR of K[La(OC$_6$H$_3$-2,6-Ph)(bdmmp)$_3$] (**5–La**) in benzene-d_6.

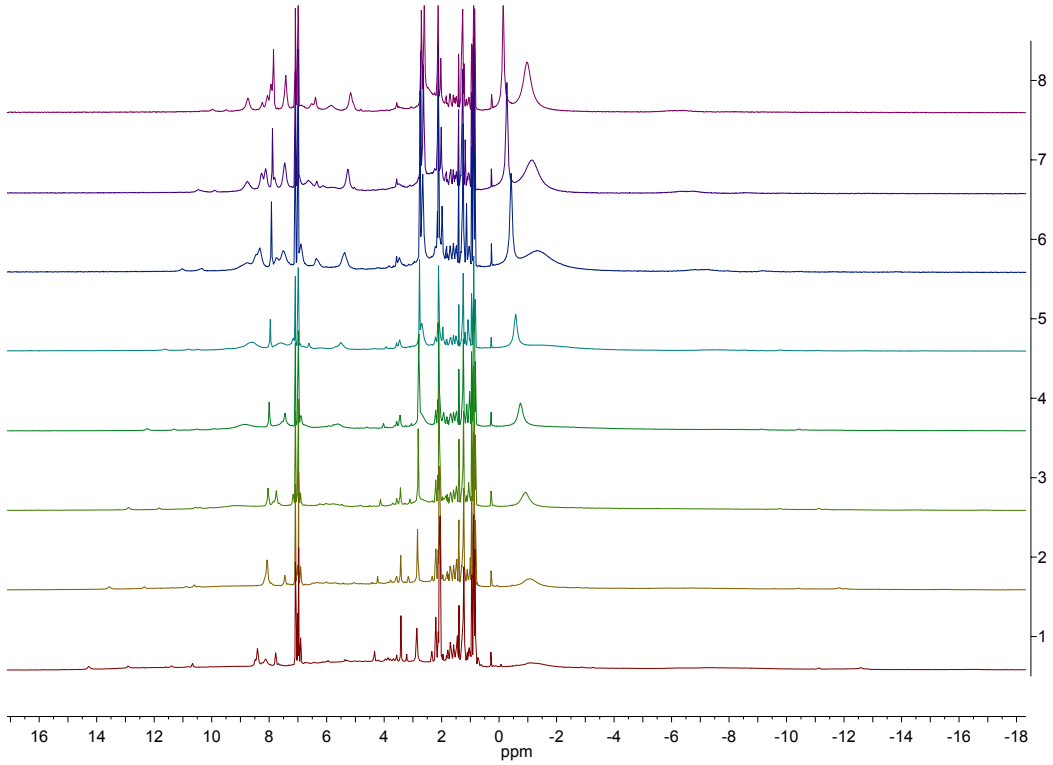

Figure S17. VT NMR of K[Ce(OC_6H_3-2,6-Ph)(bdmmp)$_3$] (**5**) in toluene-d_8 from 300–370 K.

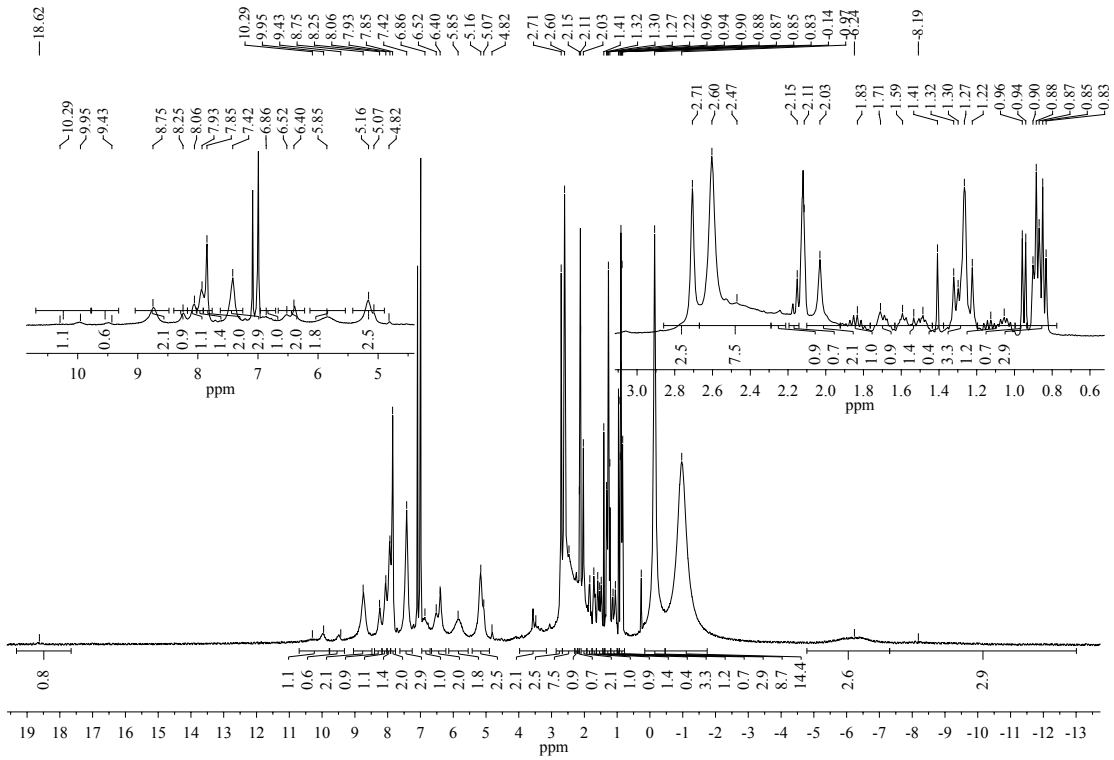

Figure S18. ^{1}H NMR of K[Ce(OC$_6$H$_3$-2,6-Ph)(bdmmp)$_3$] (**5**) in toluene-d_8 at 370 K.

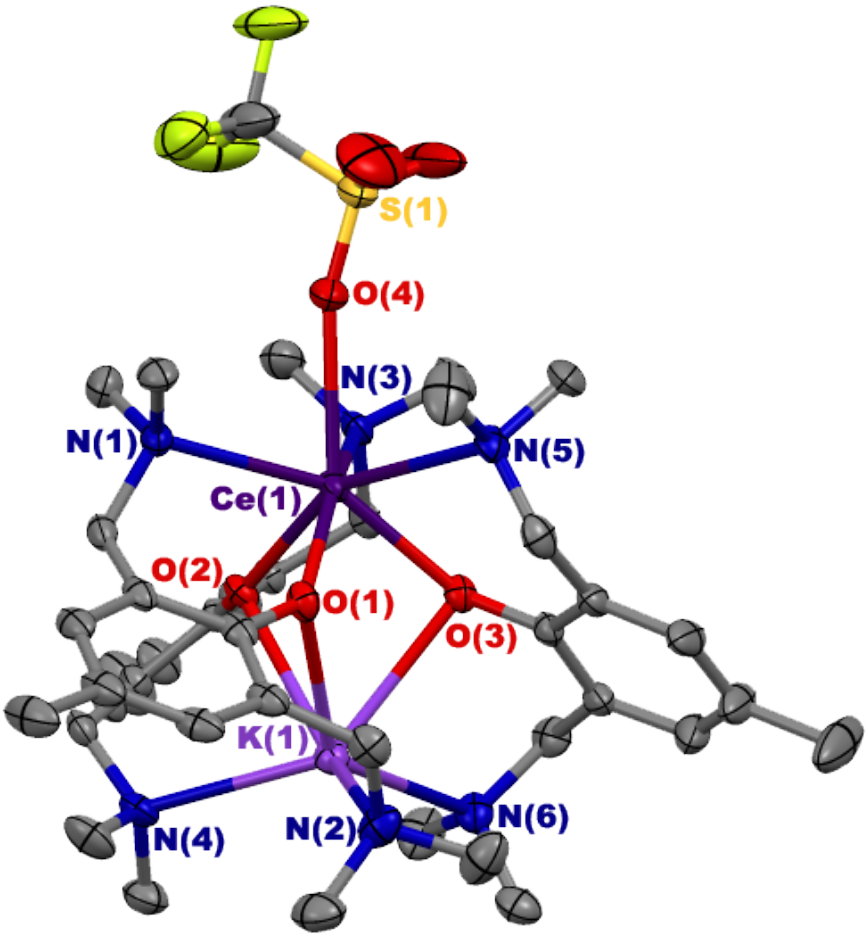

Figure S19. Thermal Ellipsoid Plot of K[Ce(OTf)(bdmmp)$_3$] (**1**) at 30 % probability. Hydrogen atoms are omitted for clarity.

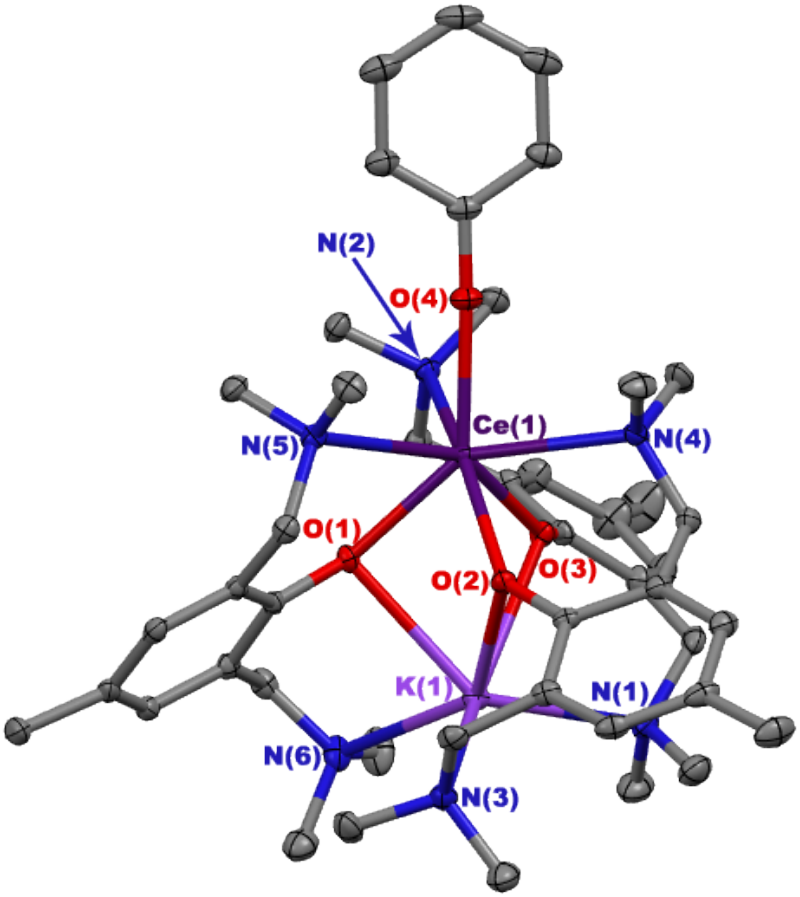

Figure S20. Thermal Ellipsoid Plot of $K[Ce(OC_6H_5)(bdmmp)_3]$ (**2**) at 30 % probability. Hydrogen atoms are omitted for clarity.

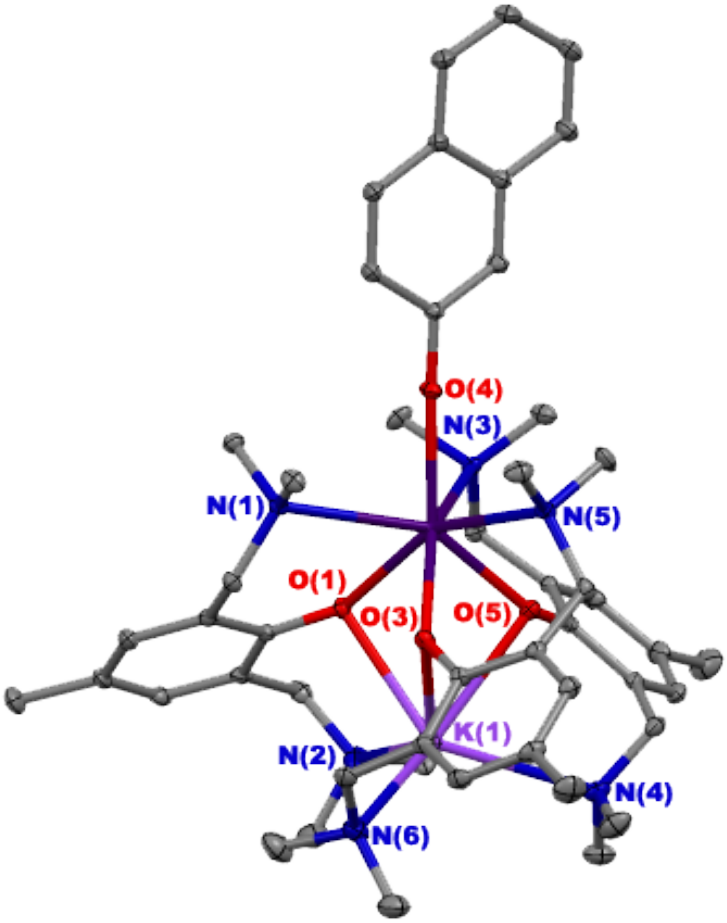

Figure S21. Thermal Ellipsoid Plot of K[Ce($OC_{10}H_7$)(bdmmp)$_3$] (**3**) at 30 % probability. Hydrogen atoms are omitted for clarity.

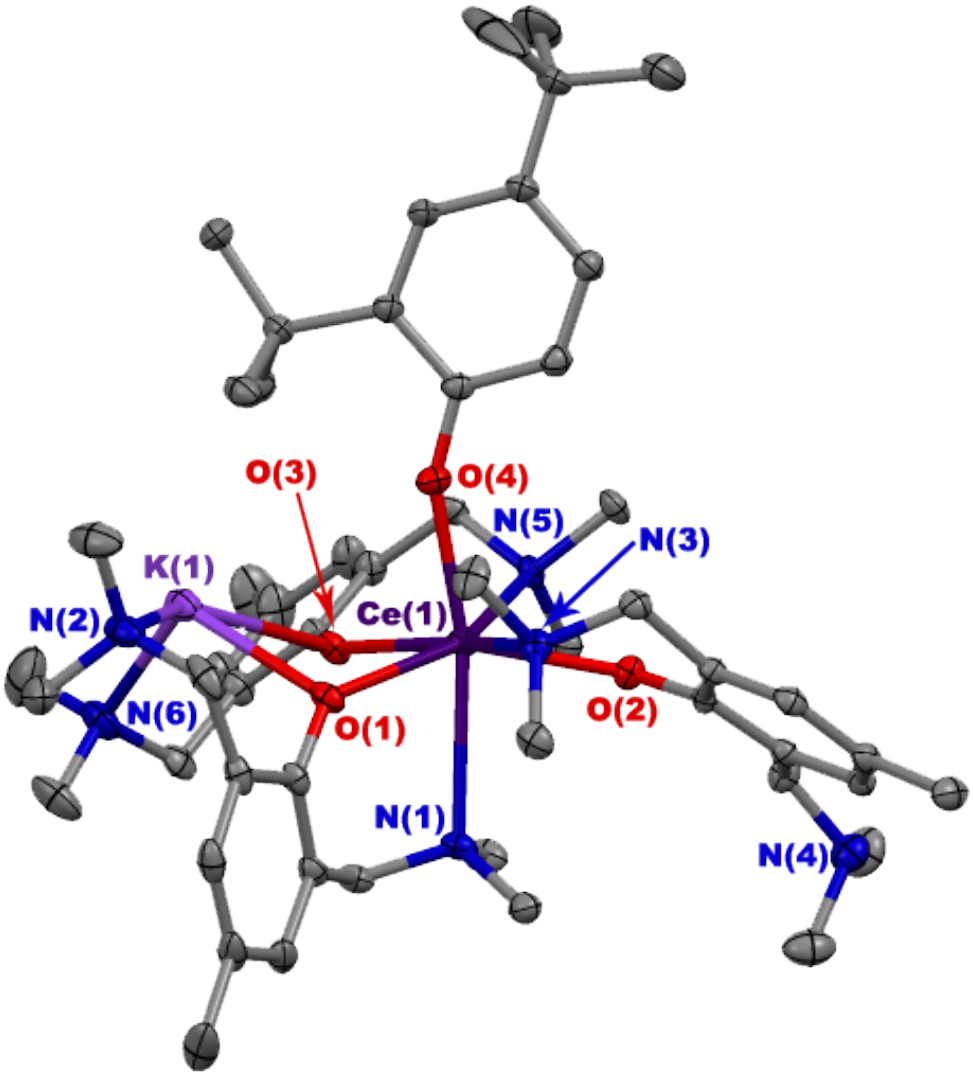

Figure S22. Thermal Ellipsoid Plot of K[Ce(OC_6H_3-2,4-*t*Bu)(bdmmp)$_3$] (**4**) at 30 % probability. Hydrogen atoms are omitted for clarity.

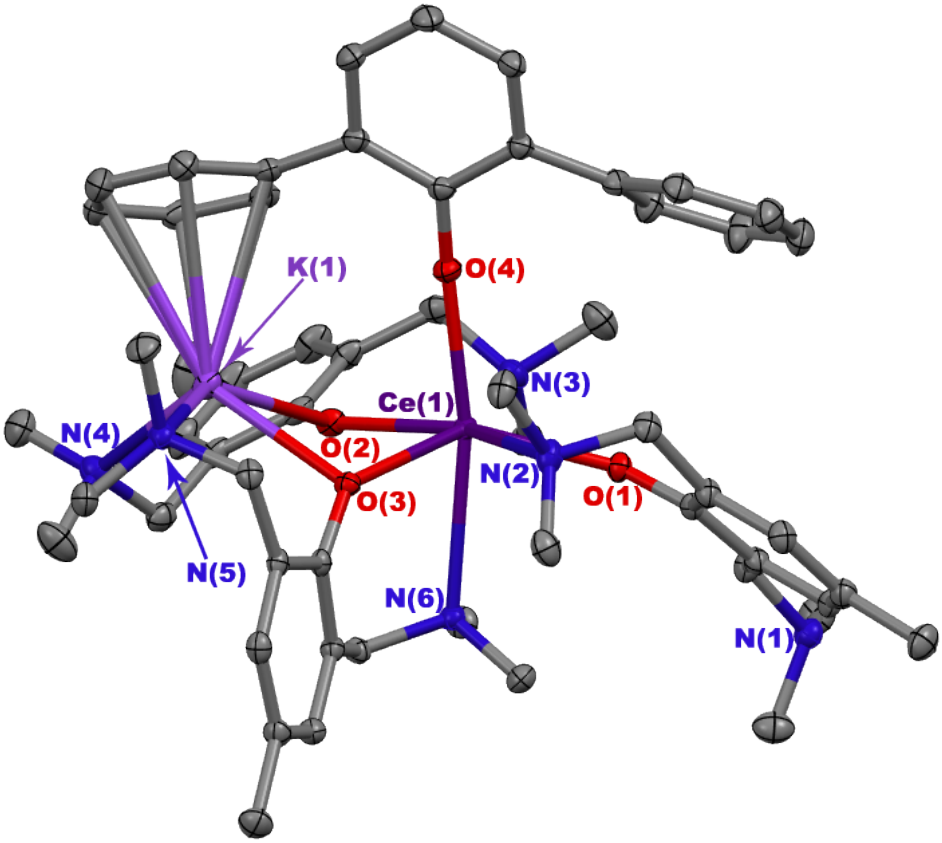

Figure S23. Thermal Ellipsoid Plot of K[Ce(OC_6H_3-2,6-Ph)(bdmmp)$_3$] (**5**) at 30 % probability. Hydrogen atoms are omitted for clarity.

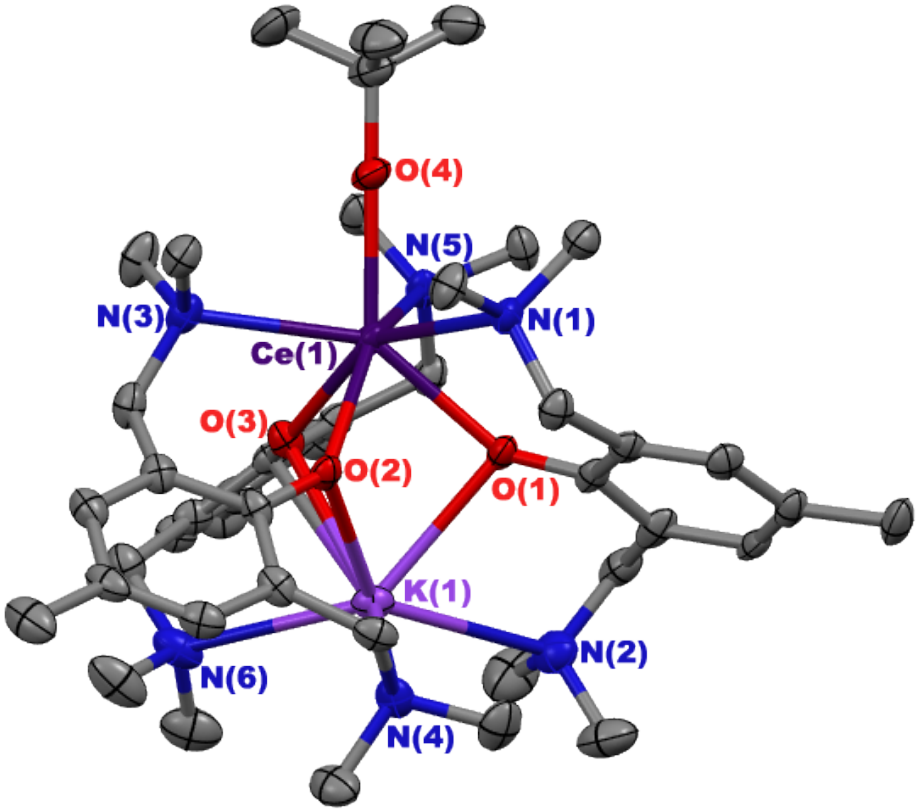

Figure S24. Thermal Ellipsoid Plot of K[Ce(O*t*Bu)(bdmmp)$_3$] (**6**) at 30 % probability. Hydrogen atoms are omitted for clarity.

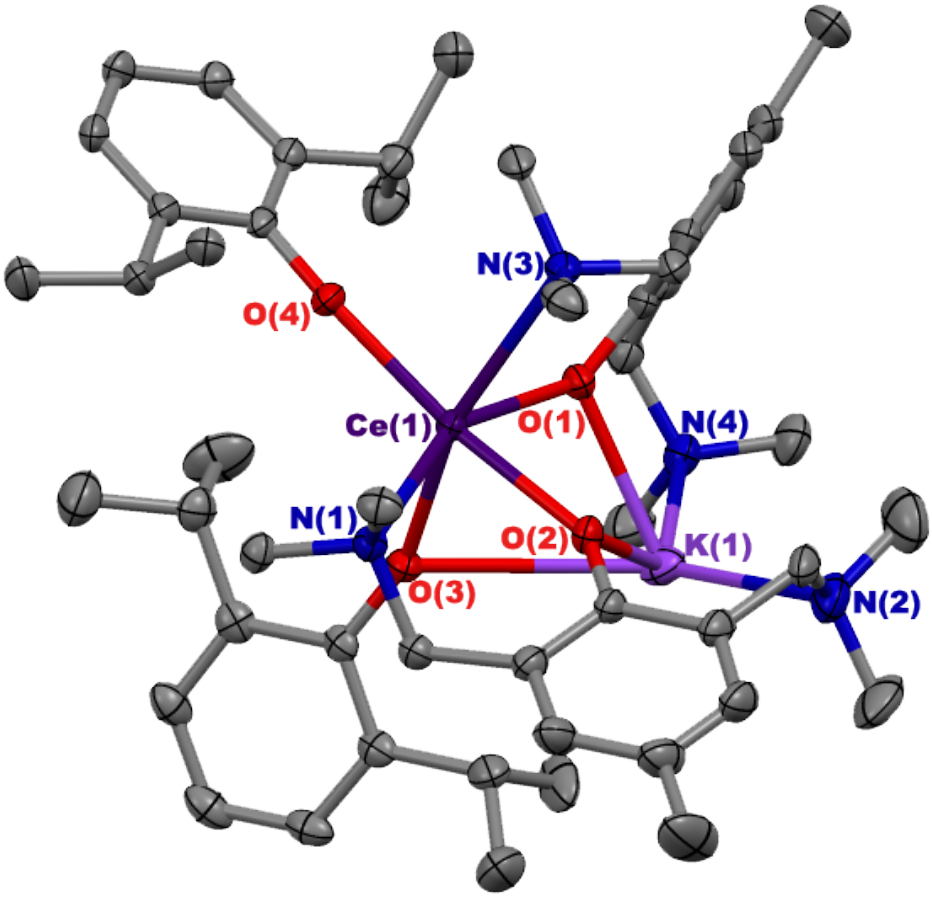

Figure S25. Thermal Ellipsoid Plot of K[Ce(OC_6H_3-2,6-*i*Pr)$_2$(bdmmp)$_2$] (**7**) at 30 % probability. Hydrogen atoms are omitted for clarity.

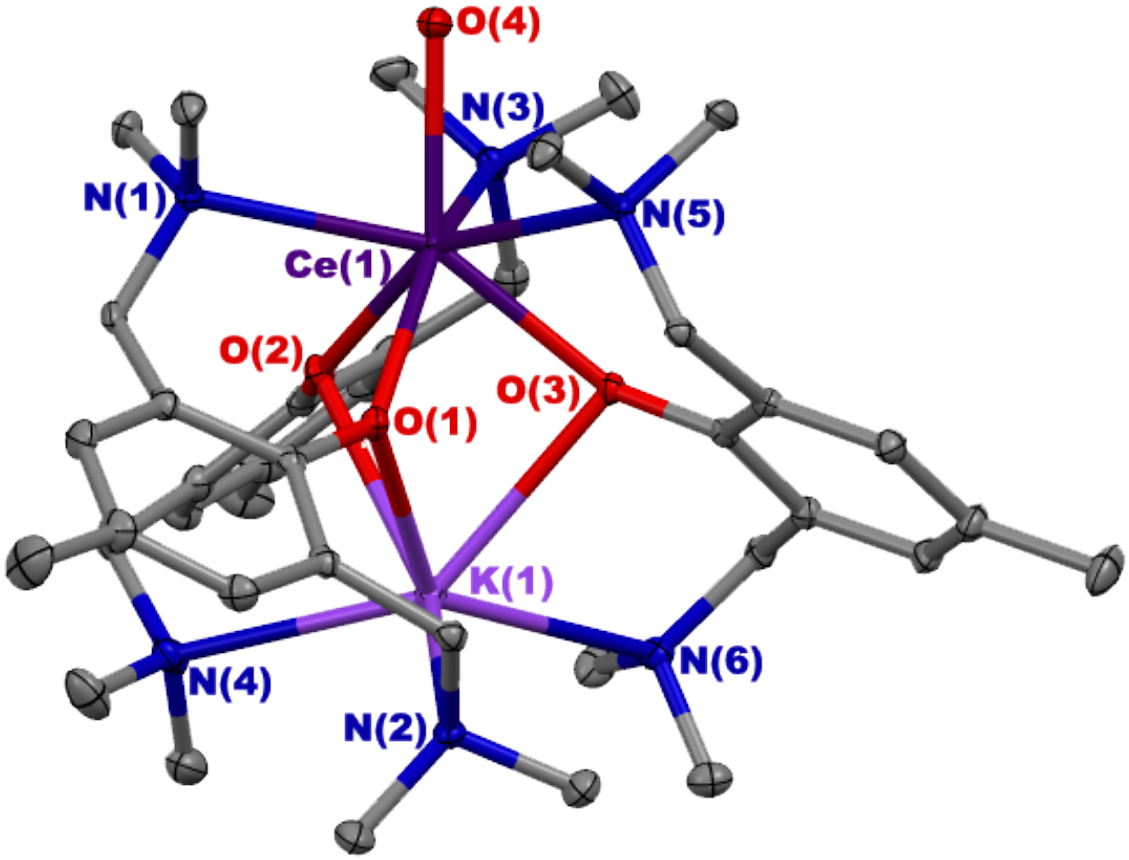

Figure S26. Thermal Ellipsoid Plot of K[Ce(OH)(bdmmp)$_3$] (**8**) at 30 % probability. Hydrogen atoms are omitted for clarity.

Figure S27a. Electrochemical Analysis of K[Ce(OC_6H_5)(bdmmp)$_3$] (**2**)

Scan rate(V/s)	sqrt. Scan rate	E_{pa} (V)	I_{pa} (A)	E_{pc} (V)	I_{pc} (A)
1	1	-0.26	-2.85E-05	-0.77	1.63E-05
0.5	0.707	-0.29	-2.13E-05	-0.75	1.36E-05
0.25	0.500	-0.32	-1.58E-05	-0.72	1.10E-05
0.1	0.316	-0.35	-1.07E-05	-0.68	8.01E-06
0.05	0.224	-0.37	-8.01E-06	-0.65	6.45E-06

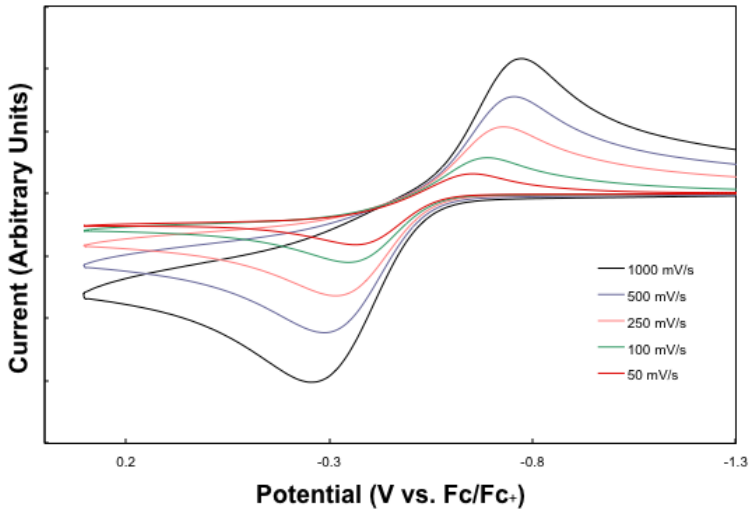

Figure S27b. Isolated $Ce^{III//IV}$ couple of **2** at scan rate dependence.

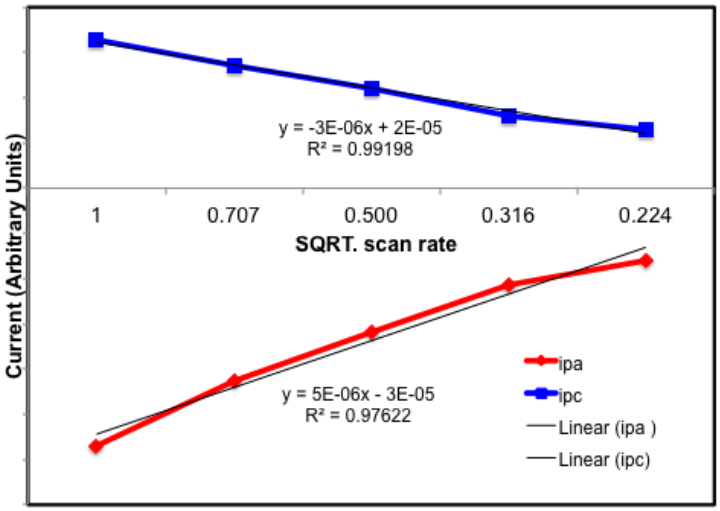

Figure S27c. The Randles-Sevcik plot of the isolated cerium(III/IV) couple of **2**.

Figure S28a. Electrochemical Analysis of K[Ce($OC_{10}H_7$)(bdmmp)$_3$] (**3**)

Scan rate(V/s)	sqrt. Scan rate	E_{pa} (V)	I_{pa} (A)	E_{pc} (V)	I_{pc} (A)
1	1	-0.22	-3.16E-05	-0.74	2.03E-05
0.5	0.707	-0.25	-2.30E-05	-0.72	1.63E-05
0.25	0.500	-0.28	-1.70E-05	-0.7	1.29E-05
0.1	0.316	-0.31	-1.14E-05	-0.66	8.66E-06
0.05	0.224	-0.34	-8.55E-06	-0.64	6.78E-06

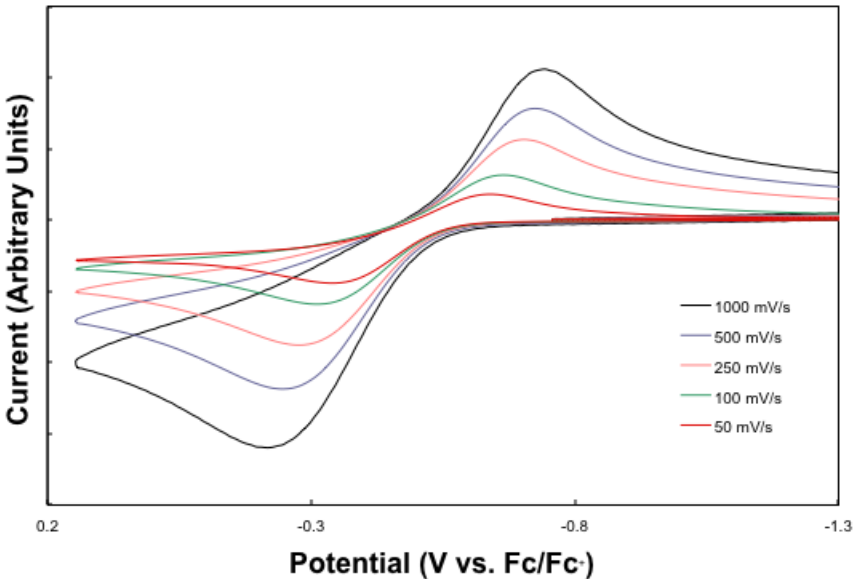

Figure S28b. Isolated $Ce^{III//IV}$ couple of **3** at scan rate dependence.

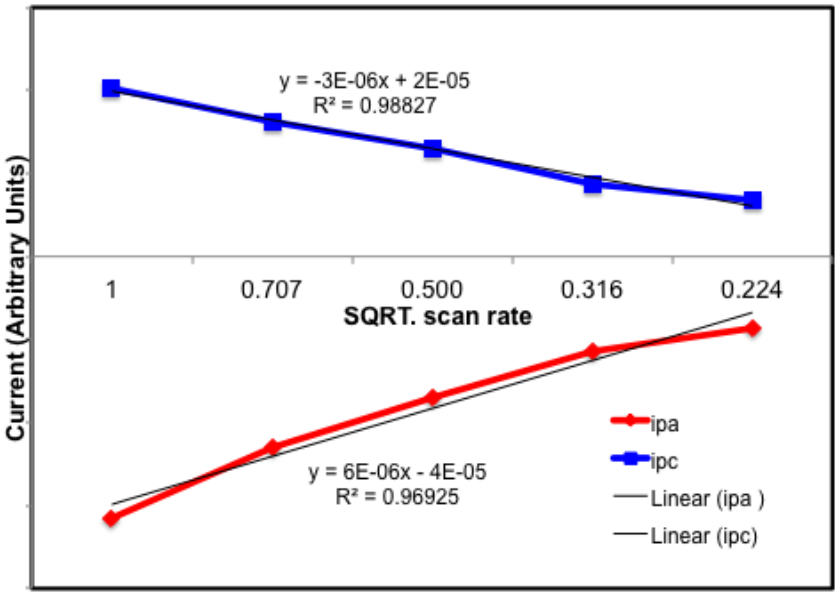

Figure S28c. The Randles-Sevcik plot of the isolated cerium(III/IV) couple of **3**.

Figure S29a. Electrochemical Analysis of K[Ce(OC_6H_3-2,4-*t*Bu)(bdmmp)$_3$] (**4**)

Scan rate(V/s)	sqrt. Scan rate	E_{pa} (V)	I_{pa} (A)	E_{pc} (V)	I_{pc} (A)
1	1	-0.18	-1.94E-05	-0.78	8.17E-06
0.5	0.707	-0.19	-1.43E-05	-0.76	5.49E-06
0.25	0.500	-0.22	-1.07E-05	-0.73	3.91E-06
0.1	0.316	-0.26	-7.11E-06	-0.69	2.78E-06
0.05	0.224	-0.28	-5.32E-06	-0.65	2.57E-06

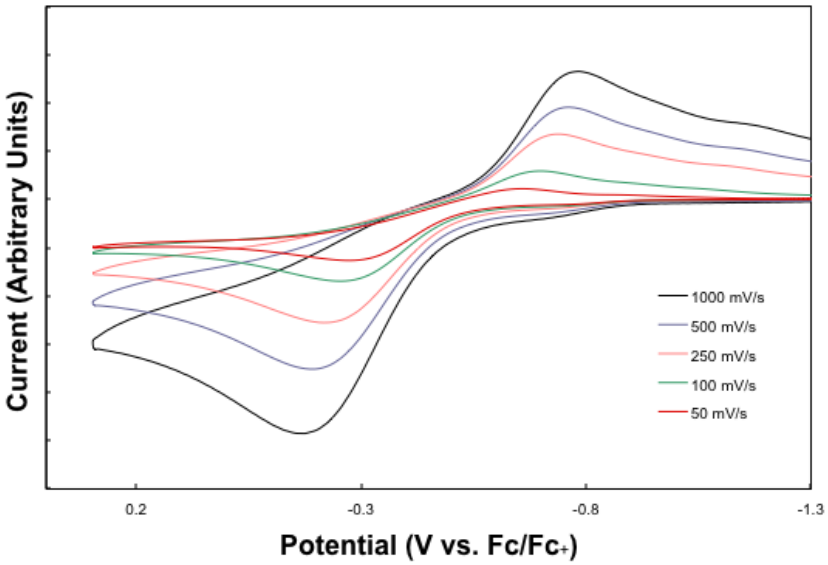

Figure S29b. Isolated $Ce^{III//IV}$ couple of **4** at scan rate dependence.

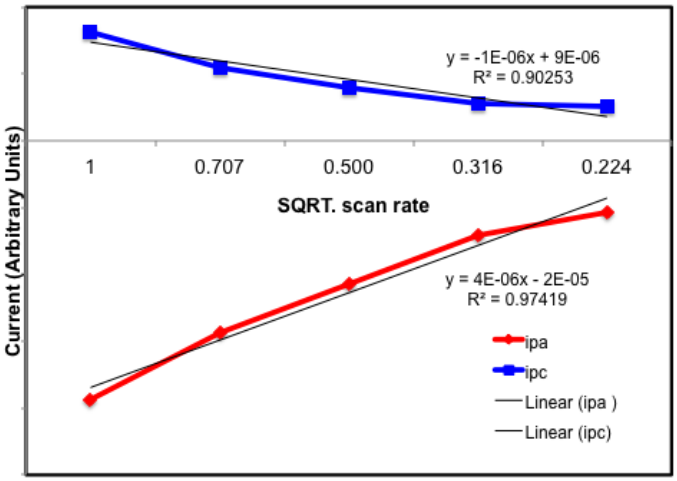

Figure S29c. The Randles-Sevcik plot of the isolated cerium(III/IV) couple of **4**.

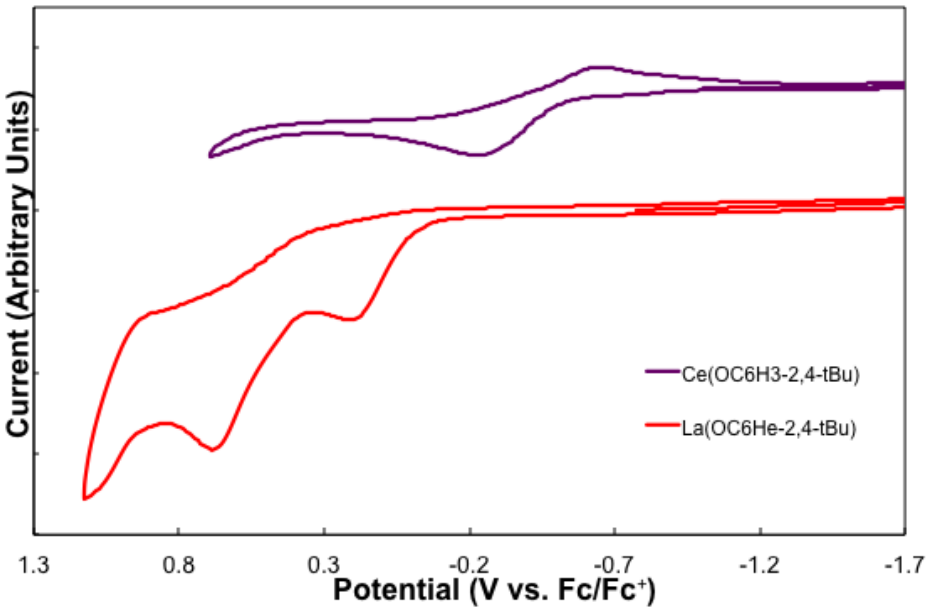

Figure S30. Cyclic voltammogram of K[Ce(OC_6H_3-2,4-*t*Bu)(bdmmp)$_3$] (**4**) and K[La(OC_6H_3-2,4-*t*Bu)(bdmmp)$_3$] (**4–La**).

Figure S31a. Electrochemical Analysis of K[Ce(OC_6H_3-2,6-Ph)(bdmmp)$_3$] (**5**)

Scan rate(V/s)	sqrt. Scan rate	E_{pa} (V)	I_{pa} (A)	E_{pc} (V)	I_{pc} (A)
1	1	-0.18	-1.94E-05	-0.78	8.17E-06
0.5	0.707	-0.19	-1.43E-05	-0.76	5.49E-06
0.25	0.500	-0.22	-1.07E-05	-0.73	3.91E-06
0.1	0.316	-0.26	-7.11E-06	-0.69	2.78E-06
0.05	0.224	-0.28	-5.32E-06	-0.65	2.57E-06

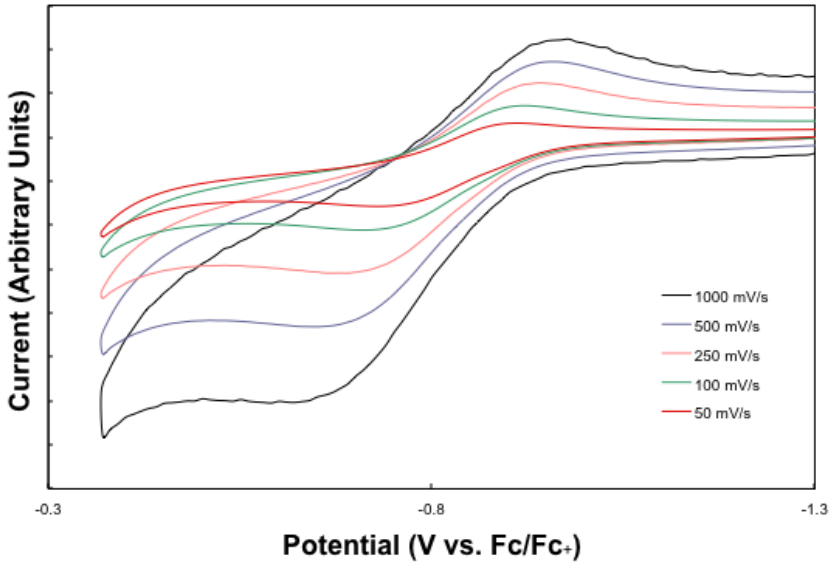

Figure S31b. Isolated $Ce^{III//IV}$ couple of **5** at scan rate dependence.

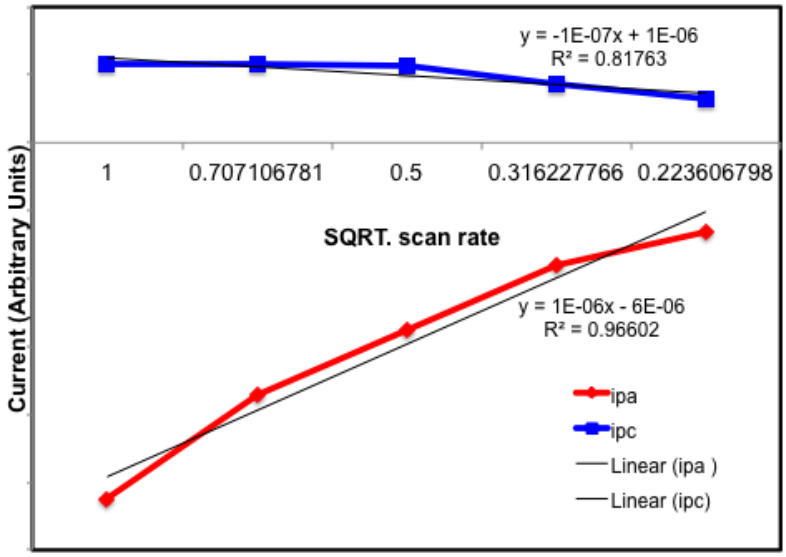

igure S31c. The Randles-Sevcik plot of the isolated cerium(III/IV) couple of **5**.

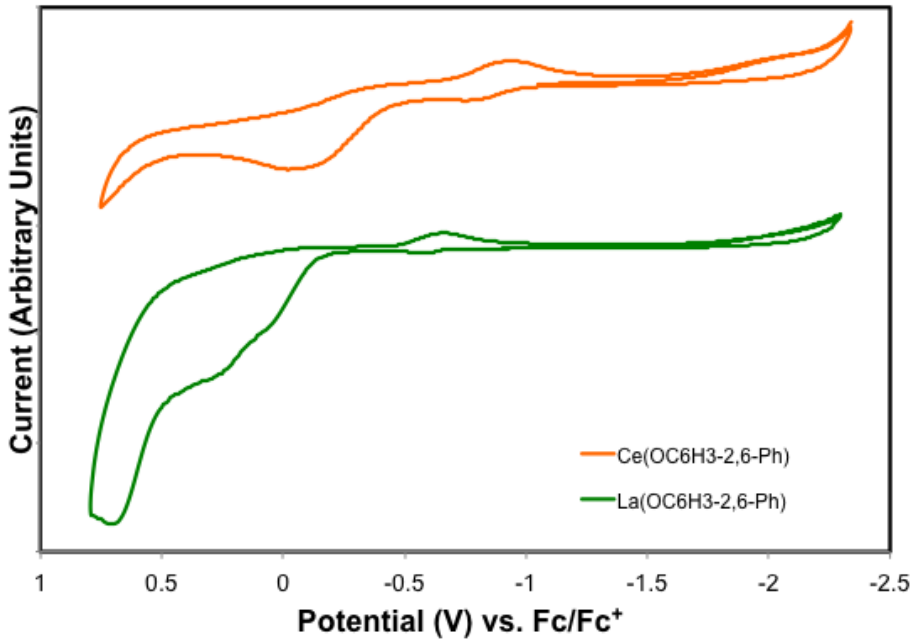

Figure S32. Cyclic voltammograms of K[Ce(OC_6H_3-2,6-Ph)(bdmmp)$_3$] (**5**) and K[La(OC_6H_3-2,6-Ph)(bdmmp)$_3$] (**5–La**).

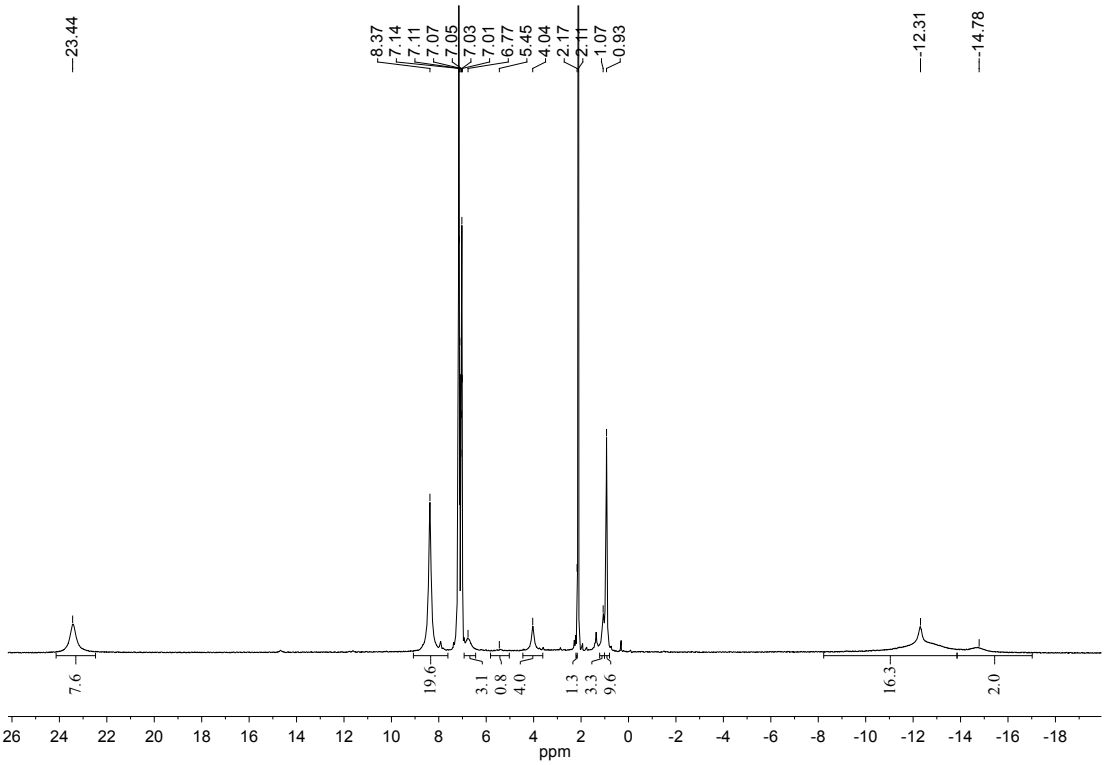

Figure S33. ^{1}H NMR of K[Ce(O*t*Bu)(bdmmp)$_3$] (**6**) in benzene-d_6.

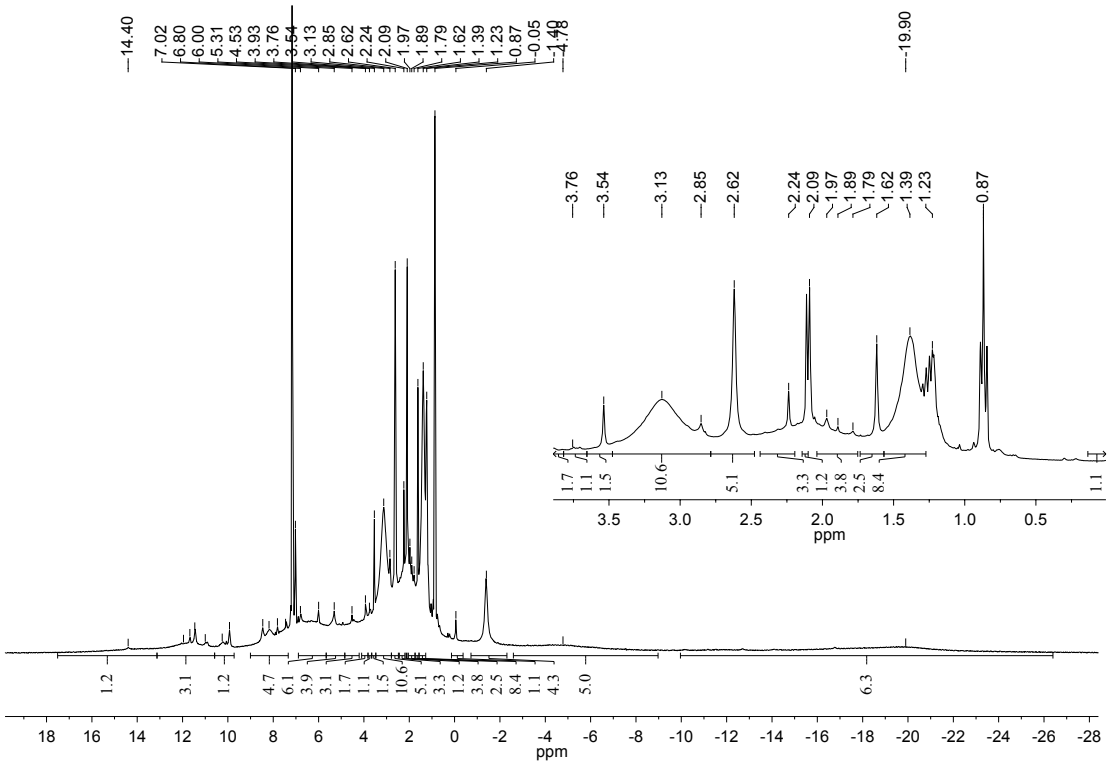

Figure S34. ^{1}H NMR of K[Ce(OC$_6$H$_3$-2,6-*i*Pr)$_2$(bdmmp)$_2$] (**7**) in benzene-d_6.

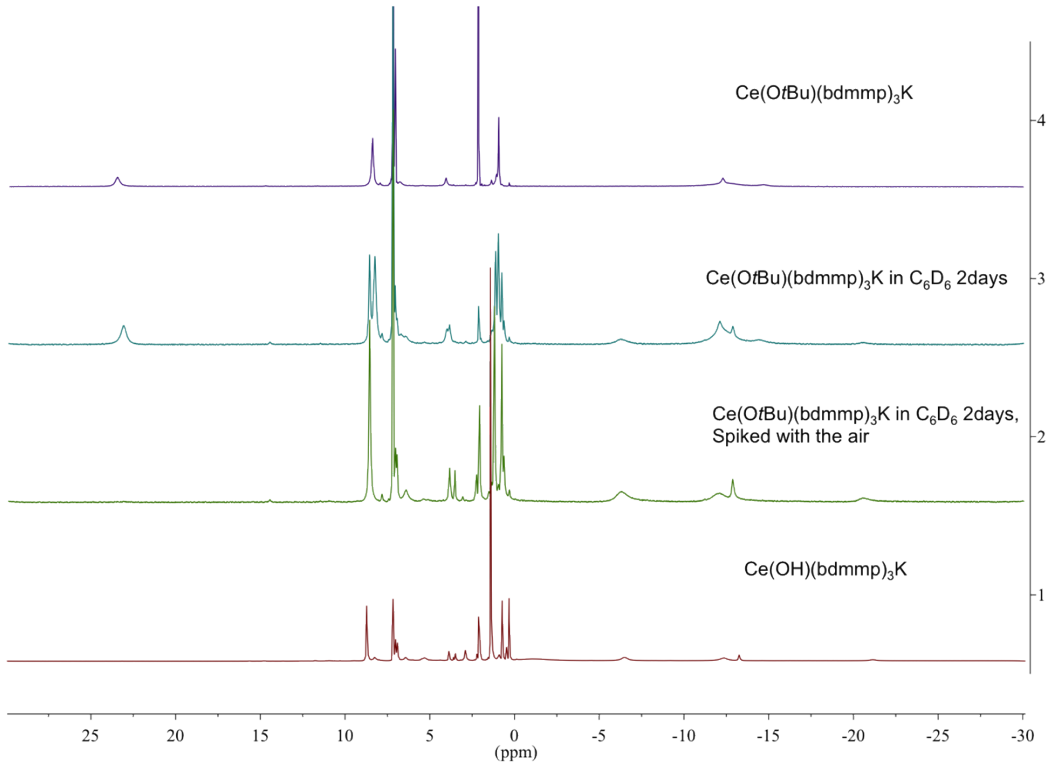

Figure S35. Decomposition of K[Ce(O*t*Bu)(bdmmp)$_3$] (**6**) to K[Ce(OH)(bdmmp)$_3$] (**8**) in glovebox.

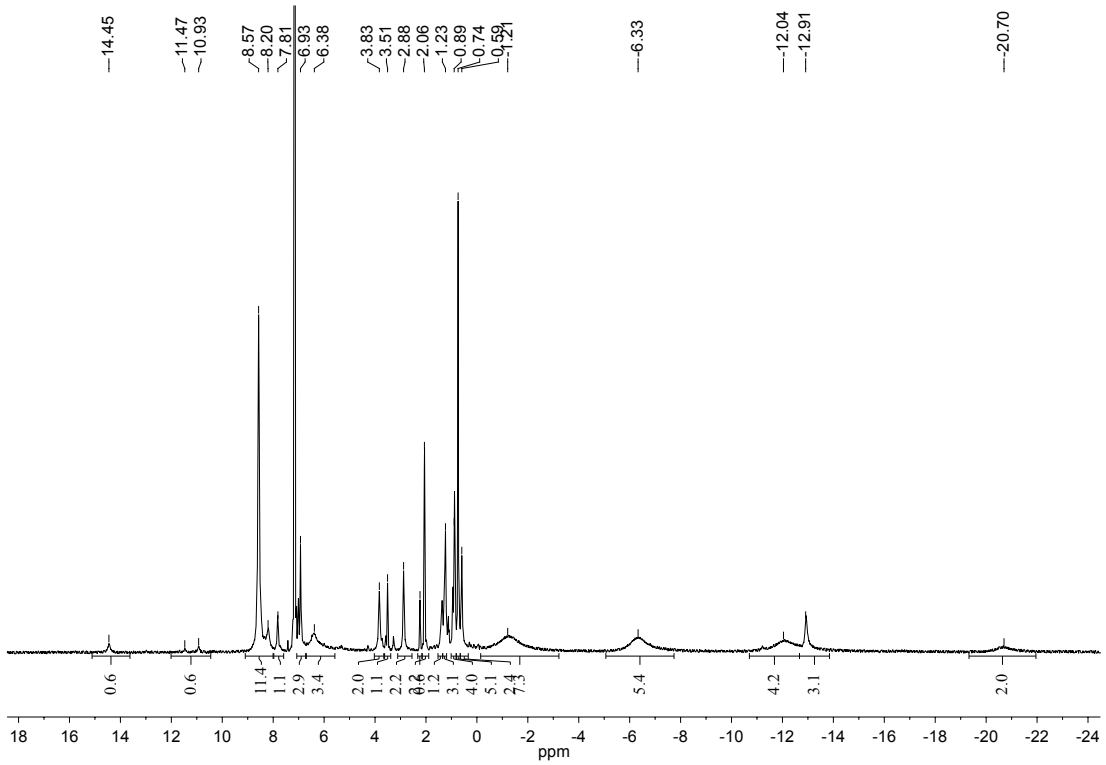

Figure S36. ^{1}H NMR of K[Ce(OH)(bdmmp)$_3$] (**8**) in benzene-d_6.

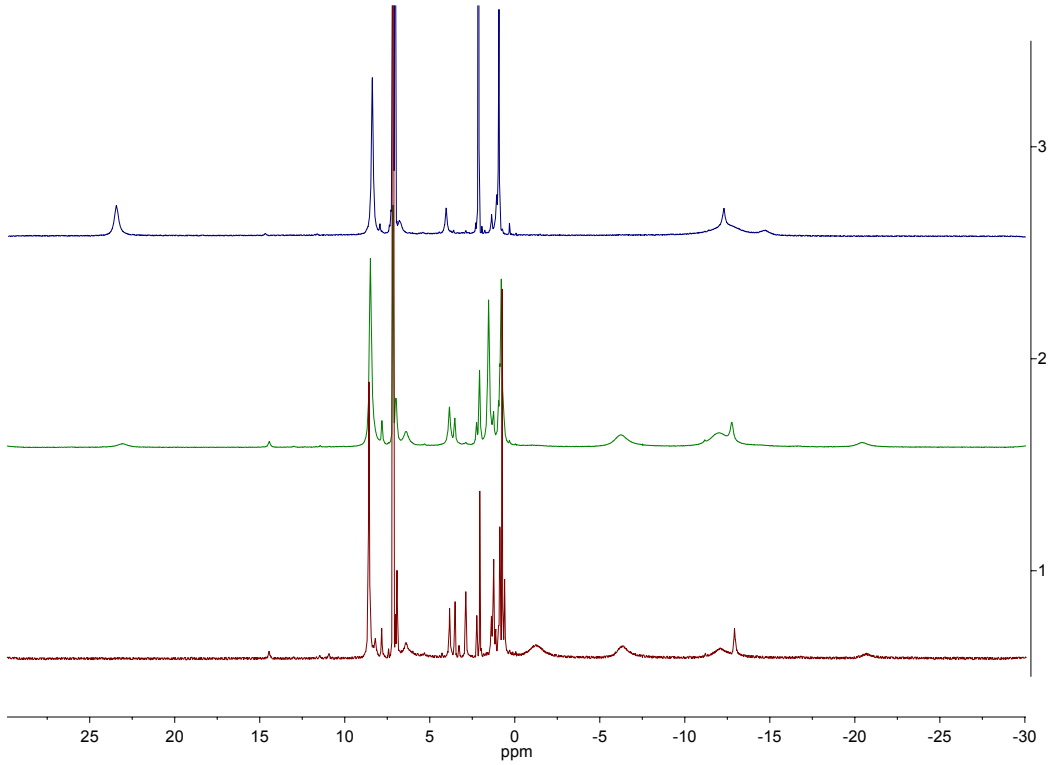

Figure S37. Addition of degassed H_2O into K[Ce(O*t*Bu)(bdmmp)$_3$] (**6**) in benzene-d_6 in the J-young tube. Top: K[Ce(O*t*Bu)(bdmmp)$_3$] (**6**), Middle: K[Ce(O*t*Bu)(bdmmp)$_3$] (**6**) + H_2O and Bottom: K[Ce(OH)(bdmmp)$_3$] (**8**)

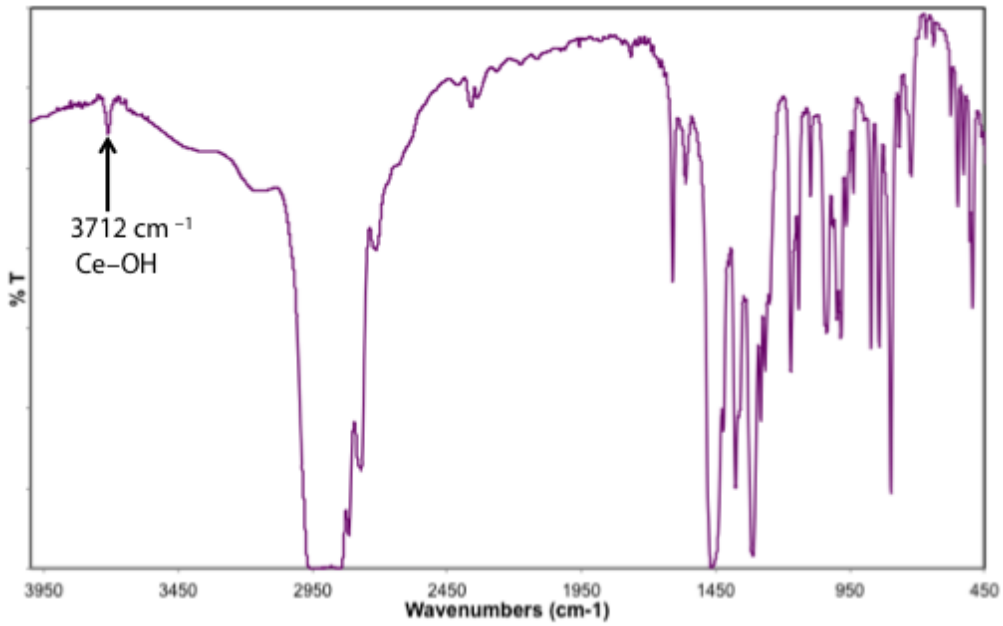

Figure S38. IR spectrum of K[Ce(OH)(bdmmp)$_3$] (**8**) in KBr plate in Nujol.

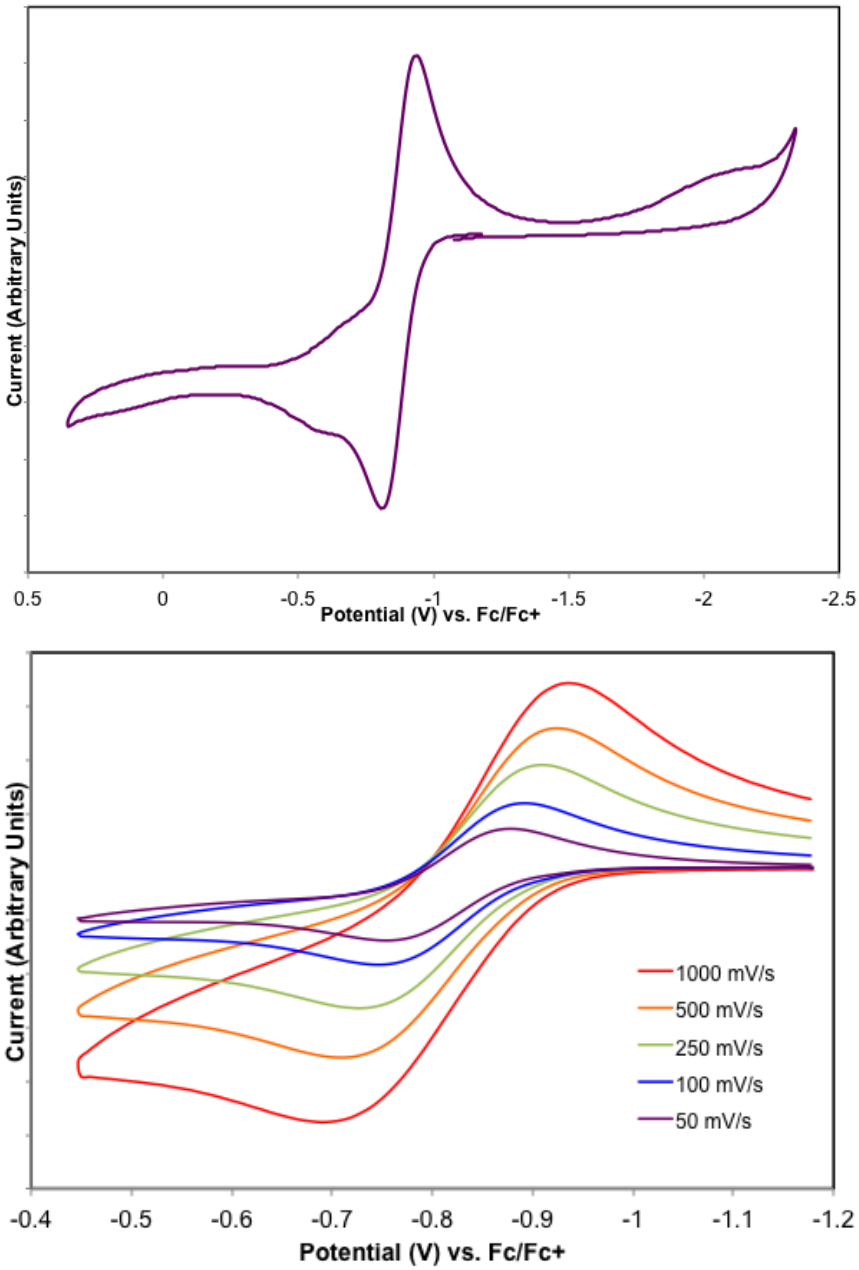

Figure S39. Cyclic voltammogram of K[Ce(OH)(bdmmp)$_3$] (**8**) in methylene chloride. (Top) full scan (bottom) isolated $Ce^{III/IV}$ couple.

Table S1. Summary of structural determination of compound **1–4**

	1	**2**	**3**	**4**
Empirical formula	$C_{61}H_{87}SN_6O_6F_3KCe$	$C_{45}H_{68}N_6O_4KCe$	$C_{63}H_{86}N_6O_4KCe$	$C_{53}H_{84}N_6O_4KCe$
Formula weight	1268.65	936.27	1170.60	1048.48
Temperature	143(1) K	143(1) K	143(1) K	143(1) K
Wavelength	0.71073 Å	0.71073 Å	0.71073 Å	0.71073 Å
Crystal system	Monoclinic	Monoclinic	Triclinic	Triclinic
Space group	$P2_1/c$	$P2_1/n$	$P\bar{1}$	$P\bar{1}$
Cell constants:				
a	20.835(3) Å	11.7314(12) Å	14.4458(9) Å	11.3184(8) Å
b	14.682(2) Å	16.3110(15) Å	14.7681(9) Å	13.5855(11) Å
c	23.143(3) Å	24.948(2) Å	15.4079(10) Å	23.2211(17) Å
α	–	–	92.430(3)°	85.902(4)°
β	115.188(6)°	97.884(5)°	91.434(3)°	76.841(4)°
γ	–	–	110.149(3)°	77.042(4)°
Volume	6406.3(15) $Å^3$	4728.7(8) $Å^3$	3080.4(3) $Å^3$	3387.5(4) $Å^3$
Z	4	4	2	2
Density (calculated)	1.315 Mg/m^3	1.315 Mg/m^3	1.262 Mg/m^3	1.028 Mg/m^3
Absorption coefficient	0.868 mm^{-1}	1.096 mm^{-1}	0.855 mm^{-1}	0.771 mm^{-1}
F(000)	2652	1956	1230	1106
Crystal size	0.35 x 0.12 x 0.10 mm^3	0.36 x 0.14 x 0.06 mm^3	0.30 x 0.12 x 0.08 mm^3	0.08 x 0.08 x 0.08 mm^3
Theta range for data collection	1.76 to 27.61°	1.50 to 27.52°	1.70 to 27.69°	1.54 to 27.66°
Index ranges	$-27 \le h \le 27$, $-19 \le k \le 19$, $-30 \le l \le 30$	$-15 \le h \le 15$, $0 \le k \le 21$, $0 \le l \le 32$	$-18 \le h \le 18$, $-18 \le k \le 19$, $-20 \le l \le 20$	$-14 \le h \le 14$, $-17 \le k \le 17$, $-30 \le l \le 30$
Reflections collected	156725	180529	126487	105132
Independent reflections	14667 [R(int) = 0.0323]	10861 [R(int) = 0.0488]	14176 [R(int) = 0.0234]	15334 [R(int) = 0.0250]
Completeness to theta = 27.59°	98.6 %	99.8 %	98.4 %	97.0 %
Absorption correction	Semi-empirical from equivalents	Semi-empirical from equivalents	Semi-empirical from equivalents	Semi-empirical from equivalents
Max. and min. transmission	0.7456 and 0.5879	0.7456 and 0.6280	0.7456 and 0.6637	0.7456 and 0.6739
Refinement method	Full-matrix least-squares on F^2	Full-matrix least-squares on F^2	Full-matrix least-squares on F^2	Full-matrix least-squares on F^2
Data / restraints / parameters	14667 / 399 / 725	10861 / 0 / 529	14176 / 0 / 692	15334 / 0 / 608
Goodness-of-fit on F^2	1.098	1.188	1.174	0.777
Final R indices [I>2sigma(I)]	R1 = 0.0611, wR2 = 0.1329	R1 = 0.0279, wR2 = 0.0732	R1 = 0.0215, wR2 = 0.0541	R1 = 0.0462, wR2 = 0.1361
R indices (all data)	R1 = 0.0798, wR2 = 0.1482	R1 = 0.0335, wR2 = 0.0750	R1 = 0.0239, wR2 = 0.0559	R1 = 0.0524, wR2 = 0.1434
Absolute structure parameter	–	–	–	–
Largest diff. peak and hole	1.348 and –1.386 $e.Å^{-3}$	0.833 and -0.863 $e.Å^{-3}$	0.635 and -0.340 $e.Å^{-3}$	1.653 and -1.032 $e.Å^{-3}$

Table S2. Summary of structural determination of compound **5–8**

	5	**6**	**7**	**8**
Empirical formula	$C_{64}H_{84}N_6O_4KCe$	$C_{43}H_{72}N_6O_4KCe$	$C_{57}H_{84}N_4O_4KCe$	$C_{99}H_{152}N_{12}O_8K_2Ce_2$
Formula weight	1180.59	916.29	1068.50	1996.76
Temperature	143(1) K	143(1) K	143(1) K	100(1) K
Wavelength	0.71073 Å	0.71073 Å	0.71073 Å	0.71073 Å
Crystal system	Triclinic	rhombohedral	Monoclinic	Triclinic
Space group	$P\bar{1}$	$R\bar{3}$	C2/c	$P\bar{1}$
Cell constants:				
a	12.1981(9) Å	49.697(5) Å Å	26.329(3) Å	10.5168(5) Å
b	13.1778(10) Å	–	14.3707(13) Å	14.2353(7) Å
c	19.5063(13) Å	10.6526(12) Å	33.138(3) Å	19.0676(10) Å
α	97.217(4) °	–	–	94.568(3) °
β	96.618(4)°	–	109.328(5)°	100.046(2)°
γ	98.276(4)°	–	–	110.486(3)°
Volume	3049.8(4) $Å^3$	22785(4) $Å^3$	11832(2) $Å^3$	2602.3(2) $Å^3$
Z	2	18	8	1
Density (calculated)	1.286 Mg/m^3	1.202 Mg/m^3	1.200 Mg/m^3	1.274 Mg/m^3
Absorption coefficient	0.865 mm^{-1}	1.022 mm^{-1}	0.883 mm^{-1}	1.000 mm^{-1}
F(000)	1238	8658	4504	1048
Crystal size	0.15 x 0.10 x 0.04 mm^3	0.12 x 0.02 x 0.01 mm^3	0.42 x 0.26 x 0.04mm^3	0.34 x 0.28 x 0.16 mm^3
Theta range for data collection	1.58 to 27.54°	1.42 to 27.52°	1.64 to 27.56°	1.55 to 27.53°
Index ranges	$-15 \le h \le 15$, $-17 \le k \le 17$, $-25 \le l \le 24$	$-64 \le h \le 63$, $-59 \le k \le 49$, $-13 \le l \le 13$	$-34 \le h \le 34$, $-18 \le k \le 18$, $-43 \le l \le 43$	$-13 \le h \le 13$, $-18 \le k \le 18$, $-24 \le l \le 24$
Reflections collected	71175	55637	103008	76235
Independent reflections	13966 [R(int) = 0.0276]	11574 [R(int) = 0.1306]	13642 [R(int) = 0.0370	11727 [R(int) = 0.0226]
Completeness to theta = 27.59°	99.4 %	99.2 %	99.7 %	97.7 %
Absorption correction	Semi-empirical from equivalents	Semi-empirical from equivalents	Semi-empirical from equivalents	Semi-empirical from equivalents
Max. and min. transmission	0.7456 and 0.6909	0.7456 and 0.6574	0.7456 and 0.6917	0.7456 and 0.6770
Refinement method	Full-matrix least-squares on F^2	Full-matrix least-squares on F^2	Full-matrix least-squares on F^2	Full-matrix least-squares on F^2
Data / restraints / parameters	13966 / 0 / 702	11574 / 0 / 515	13642 / 57 / 608	11727 / 279 / 620
Goodness-of-fit on F^2	1.061	0.800	1.287	1.088
Final R indices [I>2sigma(I)]	R1 = 0.0345, wR2 = 0.0781	R1 = 0.0649, wR2 = 0.1335	R1 = 0.0623, wR2 = 0.1331	R1 = 0.0262, wR2 = 0.0633
R indices (all data)	R1 = 0.0429, wR2 = 0.0817	R1 = 0.1606, wR2 = 0.1710	R1 = 0.0774, wR2 = 0.1386	R1 = 0.0294, wR2 = 0.0650
Absolute structure parameter	–	–	–	–
Largest diff. peak and hole	3.269 and -1.256 e.Å-3	0.652 and -0.678 $e.Å^{-3}$	1.386 and -1.614 $e.Å^{-3}$	1.057 and -0.369 e.Å-3